A STUDY ON SYMBOL SYNCHRONIZATION AND CHANNEL ESTIMATION FOR M-ARY ORTHOGONAL TRANSMISSION

A THESIS SUBMITTED TO
THE GRADUATE SCHOOL OF NATURAL AND APPLIED SCIENCES
OF
MIDDLE EAST TECHNICAL UNIVERSITY

BY

EREN KARAGÖZLÜ

IN PARTIAL FULFILLMENT OF THE REQUIREMENTS
FOR
THE DEGREE OF MASTER OF SCIENCE
IN
ELECTRICAL AND ELECTRONICS ENGINEERING

SEPTEMBER 2011

Approval of the thesis:

A STUDY ON SYMBOL SYNCHRONIZATION AND CHANNEL ESTIMATION FOR M-ARY ORTHOGONAL TRANSMISSION

submitted by **EREN KARAGÖZLÜ** in partial fulfillment of the requirements for the degree of **Master of Science in Electrical and Electronics Engineering Department, Middle East Technical University** by,

Prof. Dr. Canan Özgen
Dean, Graduate School of **Natural and Applied Sciences** _____

Prof. Dr. İsmet Erkmen
Head of Department, **Electrical and Electronics Engineering** _____

Prof. Dr. Yalçın Tanık
Supervisor, **Electrical and Electronics Engineering Dept., METU** _____

Examining Committee Members:

Prof. Dr. Mete Severcan
Electrical and Electronics Engineering Dept., METU _____

Prof. Dr. Yalçın Tanık
Electrical and Electronics Engineering Dept., METU _____

Assoc. Prof. Dr. Ali Özgür Yılmaz
Electrical and Electronics Engineering Dept., METU _____

Assoc. Prof. Dr. Çağatay Candan
Electrical and Electronics Engineering Dept., METU _____

Dr. Alime Özyıldırım
ASELSAN _____

Date: _____

I hereby declare that all information in this document has been obtained and presented in accordance with academic rules and ethical conduct. I also declare that, as required by these rules and conduct, I have fully cited and referenced all material and results that are not original to this work.

Name, Last Name: EREN KARAGÖZLÜ

Signature :

ABSTRACT

A STUDY ON SYMBOL SYNCHRONIZATION AND CHANNEL ESTIMATION FOR M-ARY ORTHOGONAL TRANSMISSION

Karagözlü, Eren

M.Sc., Department of Electrical and Electronics Engineering

Supervisor : Prof. Dr. Yalçın Tanık

September 2011, 75 pages

In this thesis, two key issues regarding M-ary orthogonal signaling systems, namely channel estimation and symbol timing recovery are investigated. Kasami codes, which are also called quasi orthogonal codes, are used for transmission of the information in place of orthogonal waveforms. In order to achieve symbol synchronization, a timing recovery scheme based on the Maximum Likelihood (ML) estimation of timing offset is proposed and the effects of proposed structure over the receiver performance are examined by using computer simulations. Moreover, the receiver performance of M-ary orthogonal signals transmitted over multipath fading channel is investigated. Least Square (LS) approach, based on the transmission of known training sequence, is used to estimate the channel impulse response. In addition to this, frame synchronization is employed at the receiver to extract the timing information by determining the start time of the received symbols. Computer simulations related to the proposed receiver structure are carried out in order to observe how the system performance is affected under multipath fading channel. Parameter selection guides regarding a good performance are also provided.

Keywords: M-ary orthogonal modulation, Kasami codes, symbol timing recovery, Least Square(LS) channel estimation, frame synchronization

ÖZ

M-ARY DİK SİNYALLERİN İLETİMİNDE SEMBOL SENKRONİZASYONU VE KANAL KESTİRİMİ ÜZERİNE ÇALIŞMA

Karagözlü, Eren
Yüksek Lisans, Elektrik ve Elektronik Mühendisliği Bölümü
Tez Yöneticisi : Prof. Dr. Yalçın Tanık

Eylül 2011, 75 sayfa

Bu tezde, M-ary dik sinyaller için kanal kestirimi ve sembol zaman bilgisinin kazanımı konuları incelenmiştir. Mesajın iletimi için dik sinyaller yerine, dike yakın kod dizisi olarak da bilinen Kasami kodlar kullanılmıştır. Sembol senkronizasyonu başarmak için en büyük olasılıklı (ML) zaman kayması kestirimi düşünülerek bir senkronizör yapısı önerilmiş ve alıcının performansı bilgisayar simülasyonları aracılığıyla analiz edilmiştir. Buna ek olarak, M-ary dik sinyallerin çok yönlü sönümlemeli kanallardan iletimi sırasındaki alıcı performansı incelenmiştir. Kanal kestirimi için bilinen ön dizilerin gönderilmesine dayanan en düşük kareler (LS) yaklaşımı kullanılmıştır. Kanal kestiriminin yanında, gerekli zaman bilgisinin belirlenmesinde alıcıya gelen sinyalin başlangıç zamanını bulan çerçeve senkronizasyonu kullanılmıştır. Önerilen alıcı yapısının performansını gözlemlemek için bilgisayar simülasyonları yapılmıştır. Ayrıca iyi alıcı performansı elde etmek için parametre seçimine yönelik yollar sunulmuştur.

Anahtar Kelimeler: M-ary dik sinyallerin iletimi, Kasami kodlar, sembol zaman bilgisinin kazanımı, En Düşük Kareler(LS) kanal kestirimi, çerçeve senkronizasyonu

To my family

ACKNOWLEDGMENTS

I would like to express my deepest gratitude to my supervisor Prof. Dr. Yalçın Tanık for his advice, criticism, encouragements, and insight throughout the research.

I would like to thank Gökhan Güvensen for his suggestions and comments.

I would also like to thank ASELSAN Inc. for the facilities provided for me to complete this thesis.

Finally, I would like to pay my sincere thanks to my parents Tülin and Sezaettin, and my dear sister Selen for their support, patience and faith to me in every aspect of life.

TABLE OF CONTENTS

LIST OF TABLES

TABLES

LIST OF FIGURES

FIGURES

CHAPTER 1

INTRODUCTION

M-ary Orthogonal modulation is a digital modulation method to transfer a digital bit stream by using M equal-energy orthogonal signal waveforms which is formed by M-dimensional signal vectors. M-ary Orthogonal modulation can ensure an increase in performance in terms of capacity. Shannon's limit is also achieved by increasing the alphabet M to infinity. The generation of M orthogonal waveforms is crucial for this modulation type. The use of spread spectrum can facilitate the generation of code sets for M-ary orthogonal modulation, since spreading codes have correlation properties similar to orthogonal codes. The use spread spectrum can also provide many advantages such as decreasing the effects of interference due to jamming, interference from other users and self interference due to the multipath propagation.

In communication systems, the transmitted signal is received at a receiver with a time delay due to the prorogation time from the transmitter to the receiver. In a digital communication system, the output of the demodulator must be sampled periodically once per symbol interval in order to recover the transmitted information. The receiver needs to know this propagation delay in order to eliminate the performance degradation due to the timing mismatch. Hence a symbol synchronization is required at the receiver. A symbol timing synchronization, which aims to estimate the time delay between the transmitted and the received signal, plays an important role in demodulation process. [11] and [17] are good references in the symbol timing synchronization literature. Symbol timing synchronization methods can be classified into two groups: Decision directed, non-decision directed methods. Decision directed methods derives the timing information by using the transmission of known symbols, whereas in non-decision directed methods the timing estimation is done without pilot known symbols.

Furthermore, multipath fading is one of major concerns in wireless communications. In a

multipath environment, the transmitted signal arrives to the receiver from different directions with a different attenuation and different time delay. Hence, the received signal is the sum of signals arriving through different propagation paths. These multiple paths cause degradation in the performance of the communication system. One approach to reduce the multipath channel effects is to detect the channel characteristics. This is accomplished by estimating the channel at the receiver. In literature, channel estimation methods are investigated in detail. [17] is good reference in the subject of channel estimation.

The aim of this thesis is to investigate the performance of M-ary orthogonal signaling. Spreading codes, such as m-sequences, Walsh Hadamard codes, Kasami codes and Gold codes are explored in order to use in M-ary signaling structure and due to better cross-correlation property Kasami codes are chosen to use in place of orthogonal signals. Initially, the performance of the proposed signaling system is explored under AWGN channel. Then the symbol timing synchronization is examined for M-ary Kasami code signaling. The symbol timing recovery scheme based on the non-decision directed approach is developed and the performance of this timing recovery scheme is analyzed by comparing with Modified Cramer Rao Bound(MCRB). Furthermore, the performance of M-ary signaling system under multipath fading channel is considered. In order to remove the multipath channel effects the proposed receiver requires the channel knowledge. For this reason, Least Square channel estimation algorithm is used in order to estimate the channel impulse response from a known training sequence. The channel estimator performance is explored for different channel responses and different training sequence lengths.

This thesis is organized is follows:

In Chapter 2, M-ary orthogonal modulation is reviewed . Then spreading codes, whose correlation properties are similar to orthogonal codes, are analyzed. Finally, the proposed receiver structure and the analyzed model is presented.

In Chapter 3, the performance of M-ary Kasami code signaling is compared with M-ary orthogonal modulation. Also Kasami codes are used in M-ary biorthogonal structure and the performance of M-ary biorthogonal signaling using Kasami codes is presented.

In Chapter 4, the proposed non-decision directed symbol synchronizer is described and the performance of this synchronizer is investigated.

In Chapter 5, transmission of M-ary signals over multipath fading channel is considered. Initially the model of multipath channel model is presented. Then, the receiver structure including frame synchronizer and Least Square channel estimator is described and simulation results related to performance of the proposed receiver structure are presented.

In Chapter 6, conclusions and possible future works are presented.

CHAPTER 2

M-ARY ORTHOGONAL SIGNALING

2.1 INTRODUCTION

Although bandwidth is a valuable commodity in wireless systems, increasing the transmit signal bandwidth can sometimes improve performance. Spread spectrum is a technique that increases signal bandwidth beyond the minimum necessary bandwidth for data communication [3]. Spread spectrum signals used for the transmission of digital information are distinguished by the characteristic that their bandwidth W is much greater than the information rate R in bits/s. In other words, the bandwidth expansion factor $B = W/R$ for spread spectrum signals is much greater than unity. Moreover, the spread spectrum modulation is performed using a spreading code, which is independent of the data in the signal. Each spreading code consists of binary-valued elements called chips with a time interval T_c. T_c should be significantly smaller than the symbol time interval T_s to satisfy the bandwidth expansion requirement. One of the most important features of spreading codes is their pseudo-randomness property which makes the signals appear similar to random noise and difficult to demodulate by the unintended receivers. Spread spectrum provides so many advantages. Some of them are as follows:

- Anti-jamming (A/J) - particularly for narrow-band jamming
- Anti-interference (A/I)
- Low Probability of Intercept (LPI)
- Multiple access capability
- Message Privacy

- High Resolution Ranging and Timing

M-ary orthogonal signaling is one of the major techniques to achieve spread spectrum. Also, the use of spread spectrum might facilitate the code generation. M-ary orthogonal signals yield a bit rate to bandwidth ratio (or spectral efficiency) of $R/W \leq 1$. Spectral efficiency decreases with increasing M. However, as M increases the SNR per bit required to achieve a given error probability decreases. Consequently, M-ary orthogonal signals are appropriate for power-limited channels which possess sufficiently large bandwidth to accommodate a large number of signals [2]. Indeed, M-ary orthogonal modulation achieves channel capacity under AWGN channel as M goes to infinity.

In this chapter, background information about M-ary orthogonal modulation is presented. Then, some spreading codes which satisfy cross correlation values similar to orthogonal codes are investigated. Finally, the investigated communication model in this thesis is presented.

2.2 LITERATURE REVIEW

In digital communication, through modulations of the carrier amplitude and phase, the constructed signal waveforms correspond to two-dimensional vectors and signal space diagrams. However it is sometimes required to construct signal waveforms corresponding to higher dimensional vectors and the number of dimension is increased by utilizing time domain or frequency domain processing or both. M-ary orthogonal signaling is a special case of multidimensional signals. M-ary orthogonal signal set consists of M equal energy orthogonal signals:

$$\int_0^T s_i(t)s_j(t)dt = \varepsilon\delta_{ij} \tag{2.1}$$

where $\delta_{ij} = 1$ when $i = j$ and zero otherwise; and ε denotes energy per symbol.

A generic form for M orthogonal signals is

$$s_i(t) = \sqrt{\varepsilon}\phi_i(t) \qquad i = 1, 2, \ldots, M \tag{2.2}$$

where ϕ_i represent orthonormal basis functions. Thus, these M orthogonal signals can be represented by $N = M$ dimensional vectors as follows:

$$\begin{aligned} s_1 &= [\sqrt{\varepsilon} \quad 0 \quad 0 \quad \dots \quad 0 \quad 0] \\ s_2 &= [0 \quad \sqrt{\varepsilon} \quad 0 \quad \dots \quad 0 \quad 0] \\ &\vdots \\ s_M &= [0 \quad 0 \quad 0 \quad \dots \quad 0 \quad \sqrt{\varepsilon}] \end{aligned} \tag{2.3}$$

The minimum distance between any two signals in M-ary orthogonal symbol set is

$$d_{ij} = \sqrt{2\varepsilon} \qquad \text{for all } i, j \tag{2.4}$$

The signal space diagrams for M=2 and N=2; M=3 and N=3 are illustrated in Figure 2.1.

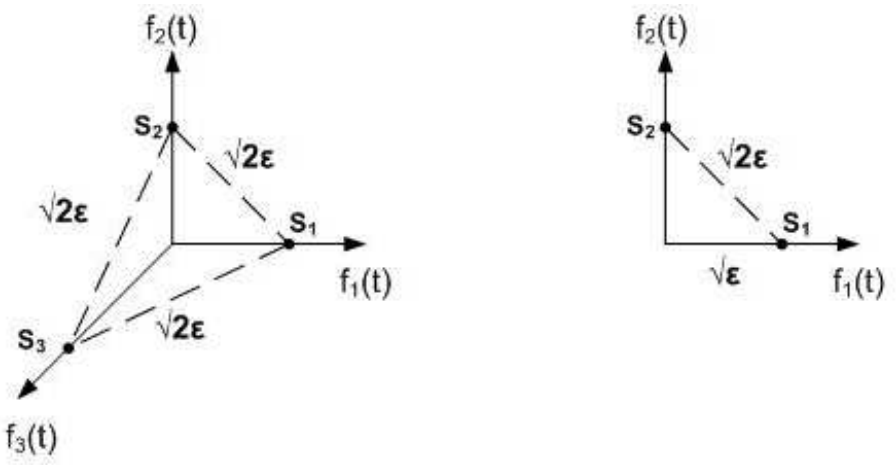

Figure 2.1: Signal space diagrams of orthogonal signals for M=N=3 and M=N=2

One way to construct orthogonal signal waveforms is to use frequency-shift-keying. This class of signals consists of sinusoids having a duration of T and signals have frequency selected from a set of M possible frequencies. The mathematical representation of these signals is [2]

$$s_i(t) = \sqrt{\frac{2E}{T}} cos[2\pi f_c t + 2\pi m \Delta f t] \tag{2.5}$$

where Δf represents the frequency difference between adjacent signals. For example, for $\Delta f = 1/2T$ the orthogonality requirement is satisfied. More details can be found in [2].

Another way to construct orthogonal waveforms is to define binary code words which are orthogonal between each other. Sample binary orthogonal code words are shown in Figure 2.2. This type of construction for M-ary orthogonal signaling is considered in this thesis.

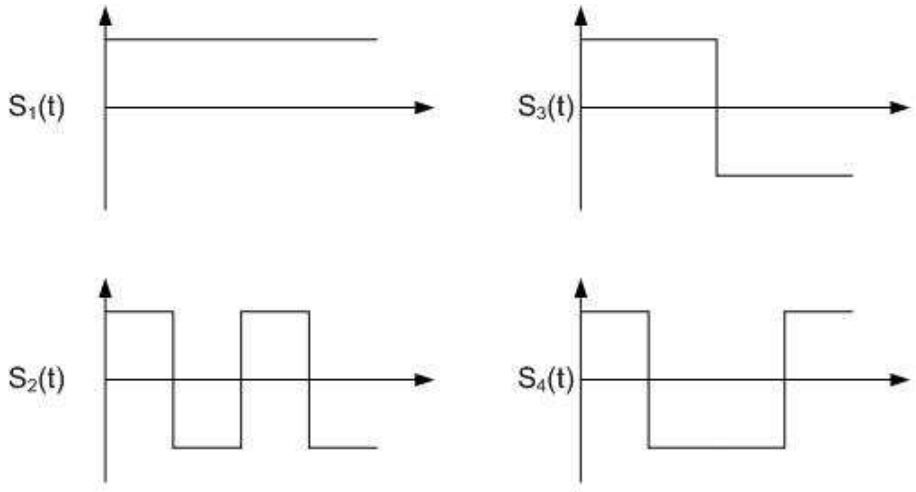

Figure 2.2: Orthogonal waveforms by using binary code words

For the detection of the transmitted signal, we use M correlators each matched to one of the possible M orthogonal signals in the receiver. Suppose the received signal is composed of signal plus noise:

$$r(t) = s_i(t) + w(t) \qquad i = 1, 2, \ldots, M \tag{2.6}$$

where $s_i(t)$ represents one of M equal energy orthogonal signals. When the received signal passes through the j-th correlator, the response of the j-th correlator to the received signal is

$$y_j = \int_0^T r(t)s_j(t)dt \qquad j = 1, 2, \ldots, M \tag{2.7}$$

$$y_j = \int_0^T s_i(t)s_j(t)dt + \int_0^T n(t)s_j(t)dt \tag{2.8}$$

This response is separated into two parts: one that results from the signal component of the received signal and one that results from the noise component of the received signal. This signal component at the j-th filter output is proportional to the signal energy and the correlation coefficient between i-th signal and j-th signal. For ideal M-ary orthogonal modulation, the correlation coefficient between any two orthogonal signals is zero. Therefore, in order to detect the transmitted signal, the optimum detector chooses the signal giving the largest cross correlation between the received signal $r(t)$ and each possible orthogonal signal $s_i(t)$.

For example, suppose s_1 is transmitted. The received signal can also be represented by the vector $\mathbf{r}$ with components r_i. Each component r_i is the projection of the received signal onto one of M possible orthogonal signals. At the input of the receiver, the received signal vector is

$$\mathbf{r} = [\sqrt{\varepsilon_s} + n_1 \quad n_2 \quad n_3 \quad \dots \quad n_M] \tag{2.9}$$

where $n_1, n_2, ..., n_M$ are zero-mean, mutually independent Gaussian random variables with variances $N_0/2$. After the received signal passes through M correlators separately, the outputs from the bank of M correlators are

$$\begin{aligned} C(\mathbf{r}, \mathbf{s_1}) &= \sqrt{\varepsilon_s}(\sqrt{\epsilon_s} + n_1) \\ C(\mathbf{r}, \mathbf{s_2}) &= \sqrt{\varepsilon_s} n_2 \\ &\vdots \\ C(\mathbf{r}, \mathbf{s_M}) &= \sqrt{\varepsilon_s} n_M \end{aligned} \tag{2.10}$$

All correlator outputs have the common factor $\sqrt{\varepsilon_s}$ and it can be eliminated from the outputs. Therefore correlator outputs are represented by the received vector $\mathbf{r} = [r_1 \quad r_2 \quad \dots \quad r_M]$. In order to make the correct decision at the receiver the related correlator output must be larger than each of other $M-1$ correlator outputs. Since s_1 is transmitted, r_1 should be larger than other correlator outputs $r_1 = \sqrt{\varepsilon_s} + n_1 > n_2, n_3 \dots, n_M$ for correct decision at the receiver. The probability that the detector makes a correct decision is expressed as follows

$$P_c = \int_{-\infty}^{\infty} P(r_1 > n_2, r_1 > n_3, \dots, r_1 > n_M | r_1) p(r_1) dr_1 \tag{2.11}$$

After some manipulations as stated in [2], the following probability of correct symbol decision is obtained

$$P_c = \int_{-\infty}^{\infty} \left(\frac{1}{2\pi} \int_{-\infty}^{r_1 \sqrt{2/N_0}} e^{-x^2/2} dx \right)^{M-1} p(r_1) dr_1 \tag{2.12}$$

The probability of erroneous symbol decision denoted by P_M is

$$P_M = 1 - P_c \tag{2.13}$$

In [2], the symbol error probability is given by

$$P_M = \frac{1}{\sqrt{2\pi}} \int_{-\infty}^{\infty} \left[1 - \left(\frac{1}{\sqrt{2\pi}} \int_{-\infty}^{y} e^{-x^2/2} dx \right)^{M-1} \right] exp \left[\frac{-1}{2} \left(y - \sqrt{\frac{2\epsilon}{N_0}} \right)^2 \right] dy \tag{2.14}$$

For M-ary signal transmission, each symbol conveys $k = log_2 M$ bits, so $\varepsilon_s = k\varepsilon_b$ where ε_b is the bit energy. Also the probability of symbol error can be expressed in terms of the bit error probability. As stated in [2], for large M the bit error probability denoted by P_b is

$$P_b \approx \frac{P_M}{2} \tag{2.15}$$

The performance of M-ary orthogonal signals can be analyzed by equation 2.14. However, when the asymptotic behaviour is considered, it is more convenient to use an upper bound on the probability of a symbol error. This upper bound can be derived by employing the union bound: The probability of error for each symbol is bounded as [2]

$$P_M \leq (M-1) Q(\sqrt{\varepsilon_s / N_0}) \tag{2.16}$$

where

$$Q(x) = \frac{1}{\sqrt{2\pi}} \int_{x}^{\infty} e^{-u^2/2} du. \tag{2.17}$$

This bound can be further simplified by upper bounding the Q-function, that is

$$Q(\sqrt{\varepsilon_s / N_0}) < e^{-\varepsilon_s / 2N_0} \tag{2.18}$$

The final form of the upper bound is

$$P_M < Me^{-\varepsilon_s/2N_0} < e^{-k(\varepsilon_b/N_0 - 2ln2)/2} \tag{2.19}$$

While $M \to \infty$, the probability of error approximates zero for $\varepsilon_b/N_0 > 2ln2 = 1.39$ or 1.42 dB. Generally the union bound is sufficiently accurate to be used as the error estimate. According to this simple upper bound, the low P_M can be satisfied as long as $\varepsilon_b/N_0 > 1.42$ dB. However, for low SNR, this bound is looser due to the assumption used for Q function in (2.18). For low SNR per bit, [2] states a tighter upper bound on P_M

$$P_M \leq 2e^{-k(\sqrt{\varepsilon_b/N_0} - \sqrt{ln2^2})} \tag{2.20}$$

Therefore, for $\varepsilon_b/N_0 > ln2 = 0.693$ or -1.6 dB, $P_M \to 0$ as $M \to \infty$. -1.6 dB is the minimum required SNR per bit to achieve a small probability of error in the limit as $M \to \infty$. This minimum SNR value is also the Shannon limit for AWGN channel which maximizes the mutual information between the input and output of the channel. Therefore, M-ary signals achieve the channel capacity bound as M goes to infinity.

2.2.1 Welch Bound

There are several bounds on the maximum cross-correlations of sequence families. One of these bounds is the Welch bound developed by Welch in 1974. Welch bound is the lower bound on the periodic cross-correlation between any pair of sequences of period N in a set of M sequences [2] and it is expressed by

$$R_{\max} \geq N\sqrt{\frac{M-1}{NM-1}} \tag{2.21}$$

where $R_{\max}$ represents the maximum cross-correlation value between any pair of sequences. For large values of N and M, the lower bound is approximated to $\sqrt{N}$.

2.2.2 PN Sequences

Pseudo noise (PN) code which is also called a pseudo random, consists of a sequence of plus or minus ones and it acts as a noiselike signal. These sequences are used for bandwidth spreading of the signal energy. This class of sequences has an important role in spread spectrum systems. There are two classes of PN sequences: periodic and aperiodic. An aperiodic sequence does not repeat itself in a periodic fashion and it is zero outside the main interval. Whereas, a periodic PN sequence is constructed by starting with a finite sequence and expanding it periodically. Periodic sequences are very important in spread spectrum systems.

Before investigating periodic sequences' properties, aperiodic sequences are reviewed briefly to point to their limits. An aperiodic sequence is described by

$$a_1 \quad a_2 \quad a_3 \quad a_4 \quad ... \quad a_N \qquad for \quad a_i = \pm 1$$

In order to classify this code as a pseudorandom code, the sequence must satisfy the autocorrelation property: The autocorrelation function of the sequence a is defined as

$$R_{aa}[k] = \sum_{n=1}^{N-k} a_n a_{n+k} \qquad k = 0, 1, ..., N-1 \tag{2.22}$$

The autocorrelation function of an ideal aperiodic sequence with length N takes following values:

$$R_{aa}[k] = \begin{cases} N & \text{if } k \equiv 0 \\ 0 \quad or \pm 1 & \text{if } k \neq 0 \end{cases} \tag{2.23}$$

For example, a Barker sequence of length $N = 11$, is

$$a[n] = [1, -1, 1, 1, -1, 1, 1, 1, -1, -1, -1]$$

The autocorrelation function corresponding this sequence is shown in Figure 2.3, satisfying the auto-correlation property.

Barker sequences are good examples of PN sequences but these codes have been discovered

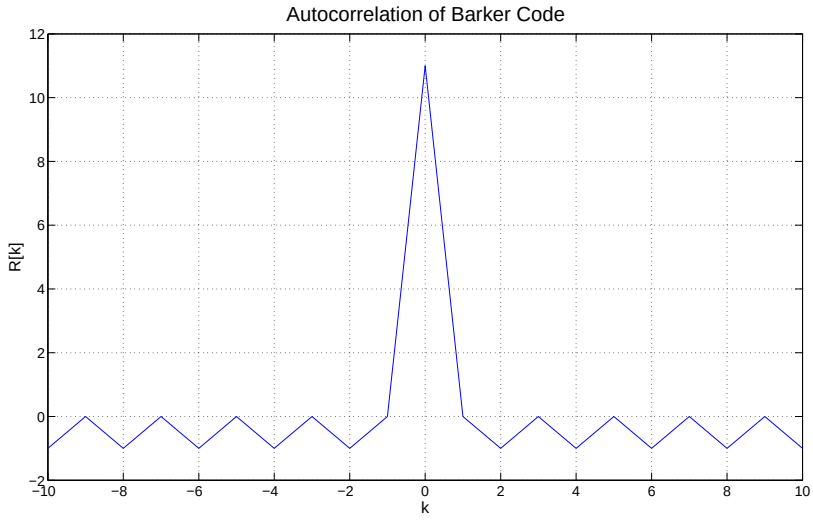

Figure 2.3: Autocorrelation of a Barker code of length 11

for only several specific sequence lengths N, namely $N = 1, 2, 3, 4, 5, 7, 11$ and 13. No larger Barker sequence has been found yet. Moreover, these sequences are generally very short for spreading purpose. However, these codes can be used for synchronization purposes. As it was stated previously, periodic sequences are much more important in spread spectrum systems. A periodic sequence repeats itself in period of N which is the length of the PN sequence and it can be illustrated by

$$...a_{N-1} \quad a_N \quad a_1 \quad a_2 \quad a_3 \quad ... \quad a_N \quad a_1... \qquad , a_i = \pm 1$$

Golomb states that such a sequence is said to be pseudorandom if it satisfies the following conditions [7], [8]:

1. **Balance property:** In each period of the sequence the number of plus ones differ from the number of minus ones by at most one. For example a sequence

   $$Pn = +1 + 1 + 1 - 1 + 1 - 1 - 1$$

   satisfies this property where the difference between plus and minus one is one.

2. **Run-length Distribution:** A run is a sequence of single type of digits. In each period one-half of the runs of each type have length 1, one-fourth have length 2, one- eighth are of length 3 and so on. Also the number of positive and negative runs must be equal.

3. **Autocorrelation:** An autocorrelation characteristic of a periodic PN sequence is its periodic autocorrelation property. The autocorrelation of a PN sequence must be two valued. The autocorrelation function of a sequence of a length N is given by

$$R_{aa}[k] = \sum_{n=1}^{N} a_n a_{n+k} \tag{2.24}$$

where $a_{n+N} = a_n$. The autocorrelation function of a periodic pseudo noise sequence is

$$R_{aa}[k] = \begin{cases} N & \text{if } k = 0 \\ -1 & \text{if } 1 \leq k \leq N-1 \end{cases} \tag{2.25}$$

For PN sequences the autocorrelation function takes the peak value only when there is a perfect synchronization between PN codes. The synchronization requirement in receiver for spread spectrum system is based on this property.

A deterministic sequence that possesses all these three properties is referred to as a pseudorandom sequence. There are different types of periodic PN sequences. The most widely known binary PN sequence is the Maximal-Length Linear Shift Register Sequence which is also called an m-sequence.

2.2.2.1 Maximal-Length Linear Shift Register Sequences (M-Sequences)

M-sequences are the most commonly used pseudorandom sequence since they are easily generated by using shift registers. Since they are also a type of cyclic codes, they are characterized by a generator polynomial. An m-stage shift register structure used to generate PN sequence is illustrated in Figure 2.4.

Feedback logic which uses taps to generate m-sequence is determined by the generator polynomial:

$$G(x) = g_m x^m + g_{m-1} x^{m-1} + g_{m-2} x^{m-2} + ... g_2 x^2 + g_1 x^1 + g_0 \tag{2.26}$$

where coefficients g_i represent tap weights and $g_0 = 1$. If g_i is equal to 1 it is connected to the feedback block. Otherwise, there is no connection. Then, modulo 2 sum of all connected feedback taps is performed and is used as the input to the shift register. This polynomial is

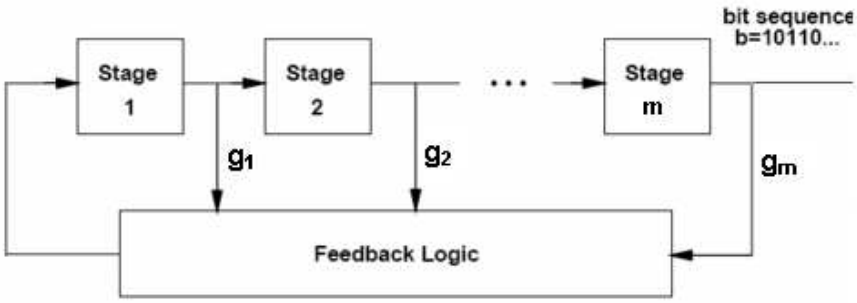

Figure 2.4: Generation of Maximal-Length Linear Shift Register Sequences

also called the feedback polynomial or characteristic polynomial. The necessary and sufficient condition for generating an m-sequence is that the generator polynomial should be primitive [16]. It is because a characteristic polynomial of degree m generates a maximal sequence of period $2^m - 1$ if and only if it is a primitive polynomial [19]. An irreducible polynomial $p(x)$ over $GF(2)$ of degree m is said to be primitive if the smallest positive integer n for which $p(x)$ divides $x^n - 1$ is $n = 2^m - 1$ [19].

An m-stage shift register has the maximum length or period

$$N = 2^m - 1 \qquad \text{where m= 1, 2, 3...} \tag{2.27}$$

The binary sequence generated from linear feedback shift register is also called a chip sequence. Then, binary elements (1,0) are mapped to the elements (1,-1), respectively. Generated m-sequences by using shift register satisfy pseudorandomness properties such as balance, run-length distribution and autocorrelation properties. The autocorrelation function of a PN sequence generated by using 5 stage shift register is shown in Figure 2.5. Since $m = 5$, the period of the sequence is $N = 31$. The autocorrelation function takes the peak value when there is no time shift. Otherwise the autocorrelation function is equal to -1.

In some applications, cross-correlation properties of PN sequences are also of interest. For multi user capabilities of spread spectrum systems, low cross-correlation values between PN codes are needed in order to minimize the interference between users. For example, in CDMA

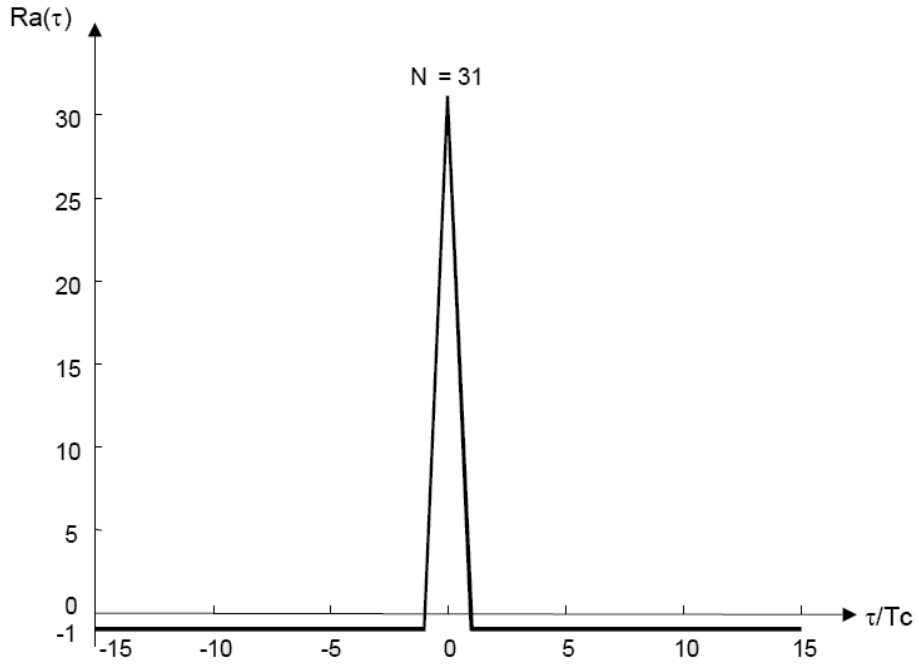

Figure 2.5: Autocorrelation of a sample m-sequence for m=5

each user owns a specified PN sequence. Ideally, the code assigned to each user should be orthogonal to others. Hence, the interference from one user to another user is zero. However, PN sequences exhibit nonzero cross-correlation values. Therefore, small correlation values are desired for multiple access techniques. When m-sequences are considered, these codes are not suitable for multi user techniques, since m- sequences can take quite large cross correlation values for some code sets. Table 2.1 gives the peak magnitude of the cross correlation between m-sequence pairs. It also shows the number of different m-sequences of length N generated by m-stage shift register.

Due to poor cross correlation properties, the maximal length sequences are not used for multi-user application. Instead of m-sequences, Gold, Kasami or Walsh codes which have much better cross-correlation properties have been developed.

2.2.2.2 Gold Codes [16]

In order to produce Gold codes, certain pairs of m -sequences called preferred sequences are used as a point of departure. Preferred sequences are m-sequences whose cross-correlation

Table 2.1: Peak cross-correlation values for m-sequences

m	$N = 2^m - 1$	Number of m-sequences	Peak cross-correaltion value R_{max}
3	7	2	5
4	15	2	9
5	31	6	11
6	63	6	23
7	127	18	41
8	255	16	95
9	511	48	113
10	1023	60	383
11	2047	176	287
12	4095	144	1407

function takes on possible values from the set ({-1,-t(m),t(m)-2}) where

$$t(m) = \begin{cases} 2^{(m+1)/2} + 1 & \text{for odd m} \\ 2^{(m+2)/2} + 1 & \text{for even m} \end{cases}$$

Gold codes are a combination of 2 preferred sequences. Although Gold codes' autocorrelation properties are worse than m-sequences, they have better cross-correlation properties than m-sequences.

Gold codes are produced by the binary addition of preferred m-sequences of length $2^m - 1$. Suppose one of preferred sequences is denoted by m-sequence1 and the other is denoted by m-sequence2 . For N cyclically shifted version of m-sequence2, a new gold code is generated by modulo two sum of sequences . Hence, N new sequences with length $2^m - 1$ are produced in total. These generated codes, which satisfy the pseudorandomness properties, are also called pseudo random sequences. Gold codes have a three-valued cross-correlation with values $(-1, -t(m), t(m) - 2)$ which are also the same as those of preferred sequences.

2.2.2.3 Kasami Codes [16]

Kasami codes are similar to Gold codes and they are also produced from m-sequences. Better cross-correlation properties can be obtained by Kasami codes. Two different sets of Kasami sequences can be generated: the small set and the large set. In order to generate the small set, firstly an m-sequence a of length $N = 2^m - 1$ is derived in which m is even and then a new sequence b is generated by sampling every $2^{m/2} + 1$ elements of a. Hence a new

sequence b is obtained with a period $2^{m/2} - 1$. Finally, the small set of Kasami sequences is generated by taking modulo 2 sum of the m-sequence a with all cyclic shifts of b. The sequence b has $2^{m-2} - 2$ cyclic shifts and by including the original m-sequence a, totally a small set which includes $2^{m/2}$ sequences is produced. The length of these sequences is $2^m - 1$. The cross-correlation and autocorrelation functions of these codes take on values from the set $(-1, -(2^{m/2} + 1), 2^{m/2} - 1)$. The larger Kasami set is also generated in a similar way as the small set. Again m-sequence a and a sequence b are produced as it is done in the generation of a small set . In addition to these sequences, a new sequence c is formed by sampling every $2^{(m+2)/2} + 1$ elements of m-sequence a. The set is then comprised by taking modulo 2 sum of a with all cyclic shifts of b and c. Therefore, a large set including more Kasami sequences is generated. The cross-correlation and autocorrelation functions of Kasami codes in the large set take on values from the set $(-1, (-1 \pm 2^{m/2}), -1 \pm 2^{m/2+1})$.

2.2.2.4 Walsh-Hadamard Codes [16]

Walsh Hadamard codes are orthogonal codes. Hence the cross correlation value of two sequences is zero when there is no time shift between sequences. The generation of Hadamard-Walsh sequences of length N is as follows.

$$H_{2N} = \begin{pmatrix} H_N & H_N \\ H_N & H_{-N} \end{pmatrix}$$

where H_N represents the Hadamard matrix. For N=2 the Hadamard matrix is

$$H_2 = \begin{pmatrix} 1 & 1 \\ 1 & -1 \end{pmatrix}$$

Each row of H_N specifies a different sequence and each sequence has a length of N. Hence we can obtain N spreading sequences which are mutually orthogonal. When synchronized, these codes have good cross-correlation property. The most distinguished disadvantage of Hadamard codes is that they are unable to satisfy the auto-correlation property.

2.3 OPTIMUM RECEIVER FOR M-ARY ORTHOGONAL SIGNALS

Suppose that the transmitted word contains N symbols and the transmitted word is expressed as

$$x(t) = \sum_{k=0}^{N-1} s_m(t - kT) \qquad m = 1, 2, \ldots, M \tag{2.28}$$

Assume that the transmitted signal is passed through a channel which is characterized by the impulse response $h_c(t)$ and corrupted by the white noise $w(t)$. Then, the received signal $r(t)$ is:

$$r(t) = \sum_{k=0}^{N-1} u_m(t - kT) + w(t) \tag{2.29}$$

where

$$u_m(t) = s_m(t) * h_c(t). \tag{2.30}$$

An optimum receiver structure for M-ary orthogonal signal set is given in Figure 2.6 [1].

As seen in Figure 2.6, the received signal is initially passed through a filter $h_c^*(-t)$ which is called the channel matched filter (CMF). Then, the CMF output is passed through a bank of M symbol matched filters (SMF), each of which is matched to the M specific signal waveforms, i.e., $s_i(t), 0 \leq t \leq T, i = 1, 2, ..., M$ and sampled periodically, once per symbol interval. Finally, the transmitted symbol is detected by picking up the symbol matched filter with the largest correlation value.

In this structure, Maximum Likelihood (ML) criterion based on the decision of the maximum of $p(r|s_m)$ is considered. Suppose the received signal is passed through the channel matched filter and the bank of M matched filters. Thus, at the output of the i-th matched filter we have

$$y_i(t) = r(t) * h_c^*(-t) * s_i^*(-t) \tag{2.31}$$

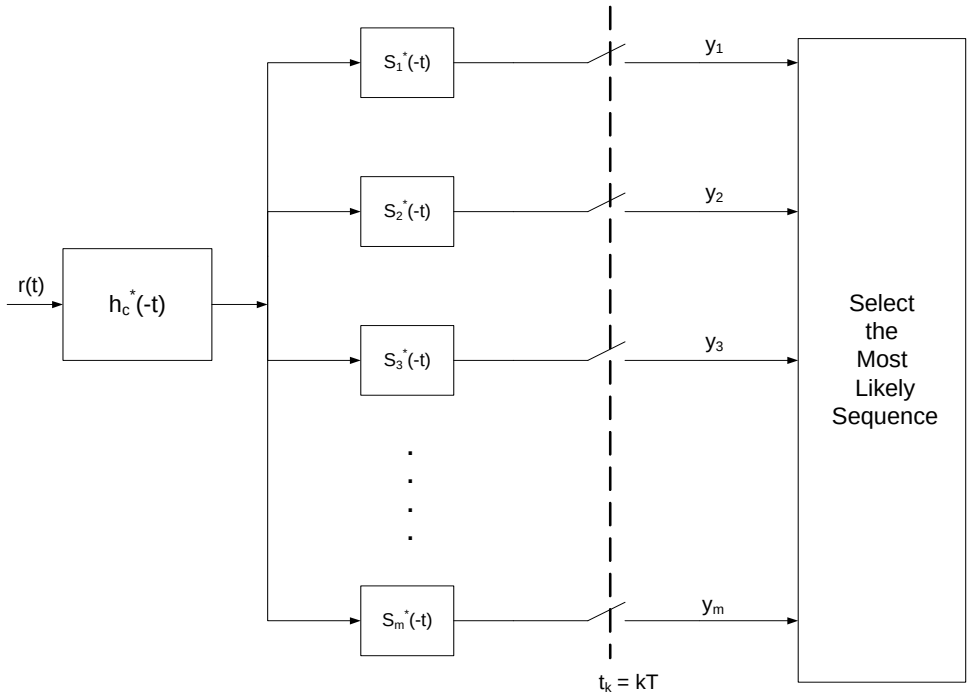

Figure 2.6: Optimum receiver block scheme

These matched filter outputs are sampled at $t = T$, the end of the symbol interval. This response can be separated into two parts: the signal component and the noise component:

$$y_i = z_i + \eta_i \tag{2.32}$$

The noise component is

$$\eta_i = w(t) * h_c^*(-t) * s_i^*(-t)|_{t=T} \tag{2.33}$$

where η_i are almost independent since s_m are nearly orthogonal. The signal component is given by

$$z_i = u_m(t) * h_c^*(-t) * s_i^*(-t)|_{t=T} \tag{2.34}$$

These terms represent the projection of the received signal onto M possible transmitted signal waveforms. Then, the outputs of the M filters are compared and the largest one is selected. This decision rule detects the signal s_m that is closest in distance to the received signal $r(t)$. It

is also referred as minimum distance detection [2].

Since the transmitted word contains N symbols, at the input of the detector, the following decision variables are produced:

$$y_i = \sum_{k=1}^{N} r(t) * h_c^*(-t) * s_{m(i)}^*(-t)|_{t=kT} \qquad i = 1, 2, \ldots, M \tag{2.35}$$

According to these decision variables, the detector estimates N symbols by picking up the symbol matched filter with a largest correlation value in each symbol interval separately.

Furthermore, it can be shown that a RAKE receiver is actually implemented by the channel matched filter: Reference [4] states that a RAKE receiver extracts multipath replicas with several correlators and performs maximum ratio combining using delay and weighting summation. It is known that a RAKE receiver features a channel matched filter which complements the channel impulse response and removes the effect of fading multipaths in a channel. Also, the CMF in this receiver structure enables the reduction of the receiver complexity and removes the channel effects as much as possible in the input of the code correlators.

2.4 THE SYSTEM STRUCTURE USED IN THIS THESIS

2.4.1 Code Selection

For exploring M-ary orthogonal signaling, practical spreading codes are used in place of orthogonal signals. There are many choices with regard to spreading sequences. In previous sections, details about spreading codes were described. In particular, the codes set size, the cross-correlation property, the sequence length are considered in the code selection to use in M-ary orthogonal signaling structure.

Now we can analyze spreading codes. It is known that for ideal orthogonal signals,

$$\sum_k s_i[k] s_j[k] = 0 \quad for \quad i \neq j \tag{2.36}$$

where $s_i[k]$ are orthogonal sequences consisting of plus and minus ones.

Walsh-Hadamard codes are orthogonal sequences. However, these codes have some draw-

Table 2.2: Comparison of Orthogonal, Kasami and Gold codes

Code Type	Length	Constraint of m	Code Set Size	R_{max}
Orthogonal Sequences	N.A.	N.A.	N.A.	0
Gold Sequences	$2^m - 1$	m odd	$2^m + 1$	$2^{(m+1)/2} + 1$
Gold Sequences	$2^m - 1$	m even	$2^m + 1$	$2^{(m+2)/2} + 1$
Large set of Kasami Sequences	$2^m - 1$	m even	$\approx 2^{3m/2}$	$2^{m/2+1} + 1$
Small set of Kasami Sequences	$2^m - 1$	m even	$2^{m/2}$	$2^{m/2} + 1$

backs: Although the full-sequence cross-correlation is identically zero, this does not hold for partial sequence cross-correlation function. Moreover, these codes possess poor auto-correlation property. These codes can easily be affected by multipath channel which results in interference. The consequence is that the advantage of using orthogonal codes is lost.

The other spreading codes examined in the previous sections are not orthogonal but they possess good correlation properties. Hence, we can consider to use these codes in place of orthogonal signals. Possible spreading codes mentioned in previous sections are Barker codes, m-sequences, Gold codes and Kasami codes. Barker codes are not suitable for M-ary orthogonal signal structure because there are only one sequence for each length. M-sequences have worse cross-correlation properties than Gold and Kasami codes. Table 2.2 compares Kasami, Gold codes with ideal orthogonal codes in terms of the sequence length, code set size and maximum cross-correlation value.

The Welch lower bound is approximated to $R_{max} \geq \sqrt{N}$ when N and M is large. For Gold and Kasami sequences, $N = 2^m - 1$ and the bound becomes

$$R_{max} \approx 2^{m/2} \tag{2.37}$$

As seen in table 2.2, the peak cross-correlation value for Gold codes is larger by $\sqrt{2}$ for odd m and by 2 for even m in comparison to Welch lower bound. Furthermore, for the large set of Kasami sequences, the peak correlation value between any pair in this set is larger than Welch lower bound. However, the maximum cross-correlation value for codes in a small set of Kasami sequences is

$$R_{max} = 2^{m/2} + 1 \tag{2.38}$$

This value approximately satisfies the Welch lower bound, so it may be stated that Kasami codes are the best choice. Therefore, the small set of Kasami sequences is employed as M-ary code set in our work.

2.4.2 Kasami Code Generation

In the previous section, the small set of Kasami codes has been chosen for M-ary signaling structure. In this work, we choose $M = 8$. A small set of Kasami codes produced from an m-sequence, has $2^{m/2}$ members. Since 8 Kasami sequences are generated, the number of stage of the m-sequence is

$$m = 6$$

and the length of each Kasami code is

$$N = 2^m - 1 = 63$$

Firstly, an m-sequence must be produced to generate Kasami codes. The m-sequence is derived from the linear shift register with feedback taps determined by a generator polynomial that must be primitive. Some primitive polynomials for the order $m = 6$ are as follows

$$\begin{gathered} x^6 + x + 1 \\ x^6 + x^5 + 1 \\ x^6 + x^5 + x^4 + x + 1 \end{gathered} \tag{2.39}$$

In this work, we choose

$$G(x) = x^6 + x^5 + 1 \tag{2.40}$$

The linear feedback shift register corresponding to the generator polynomial expressed in equation 2.40 is shown in Figure 2.7.

By using this shift register model, an m-sequence, called *a*, is generated. 7 more sequences must be generated for a small set of Kasami sequences. By following the procedures in section 2.2.2.3, firstly a new sequence *b* is generated by sampling every 9 elements of the m-sequence

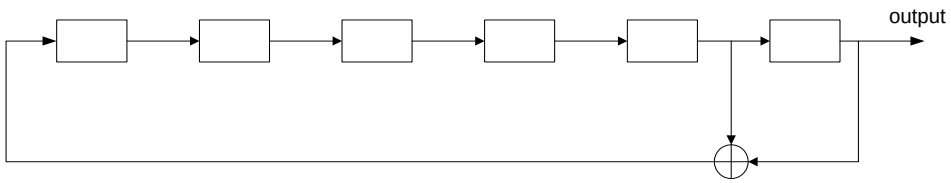

Figure 2.7: Linear feedback shift register for related polynomial

a. Then, other 7 elements of the small set are generated by taking modulo 2 sum of the m-sequence *a* with all cyclic shifts of *b*. The generated Kasami sequences are shown in table 2.3.

The auto-correlation of the m-sequence *a* is shown in Figure 2.8. Since the sequence *a* is an original m-sequence, the auto-correlation function only takes on values 63, the length of the m-sequence, and -1 as shown in this figure. Also, some auto-correlation and cross-correlation functions of the generated Kasami sequences are shown in Figures 2.9 and 2.10. It can easily be observed that the cross-correlation and auto-correlation functions of Kasami sequences take on values from the set (-1,-9,7). However, these calculations are conducted by considering that the generated Kasami sequences with a length of 63 are periodic, that is, the sequence is repeated periodically. However, it is not realistic to consider the sequence to be periodic. Therefore, we consider the generated Kasami sequences in an aperiodic fashion, that is to say, generated finite sequences are not repeated periodically. The auto-correlation and cross-correlation functions corresponding to aperiodic Kasami sequences are shown in Figures 2.11 and 2.12. It is observed that the auto-correlation and cross-correlation functions also take low values, the maximum value being 13.

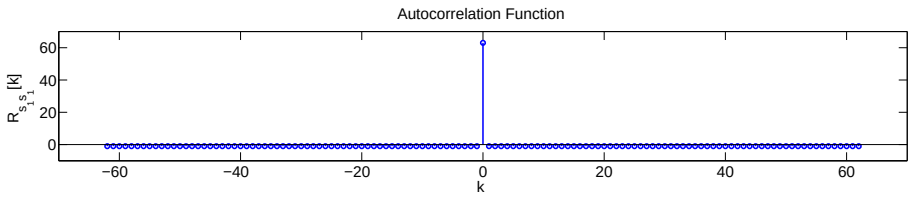

Figure 2.8: Autocorrelation function of the generated m-sequence *a*

Table 2.3: Generated Kasami sequences of length $N = 63$

No	Generated Kasami Sequences
1	1, -1, -1, -1, -1, -1, 1, -1, -1, -1, -1, 1, 1, -1, -1, -1, 1, -1, 1, -1, -1, 1, 1, 1, 1, -1, 1, -1, -1, -1, 1, 1, 1, -1, -1, 1, -1, -1, 1, -1, 1, 1, -1, 1, 1, 1, -1, 1, 1, -1, -1, 1, 1, -1, 1, -1, 1, -1, 1, 1, 1, 1, 1
2	1, -1, 1, 1, 1, -1, -1, -1, -1, 1, 1, -1, 1, 1, -1, -1, -1, 1, -1, -1, 1, 1, 1, -1, -1, 1, 1, 1, -1, -1, -1, -1, -1, -1, 1, 1, -1, 1, -1, 1, 1, -1, -1, 1, -1, -1, 1, 1, -1, -1, -1, -1, -1, 1, 1, 1, 1, -1, -1, -1, -1, 1, -1
3	1, 1, 1, 1, -1, 1, 1, -1, 1, 1, 1, 1, -1, -1, -1, 1, -1, 1, 1, 1, -1, 1, -1, -1, -1, -1, -1, -1, -1, 1, -1, -1, 1, 1, -1, 1, 1, 1, -1, -1, -1, 1, -1, -1, -1, -1, -1, -1, 1, -1, 1, -1, -1, -1, -1, 1, 1, -1, -1, 1, -1, 1
4	-1, 1, 1, -1, 1, -1, 1, 1, 1, 1, -1, -1, 1, -1, 1, 1, -1, -1, -1, -1, -1, -1, -1, -1, 1, 1, 1, -1, 1, 1, -1, 1, -1, -1, -1, -1, 1, 1, 1, 1, 1, 1, 1, -1, -1, 1, 1, 1, 1, 1, 1, -1, 1, 1, 1, -1, -1, 1, -1, 1, -1, 1, 1
5	-1, 1, -1, 1, -1, -1, -1, 1, 1, -1, 1, 1, 1, 1, 1, 1, 1, 1, 1, -1, 1, -1, -1, 1, -1, -1, 1, 1, 1, 1, 1, -1, 1, -1, 1, -1, 1, -1, -1, -1, 1, -1, 1, -1, 1, -1, -1, 1, -1, 1, 1, 1, -1, -1, 1, 1, -1, 1, 1, -1, 1, 1, -1
6	-1, -1, 1, -1, -1, 1, -1, 1, -1, 1, -1, 1, -1, 1, 1, -1, -1, -1, 1, 1, 1, -1, 1, -1, 1, -1, -1, 1, 1, -1, -1, 1, 1, 1, 1, -1, -1, 1, 1, -1, -1, -1, 1, 1, -1, 1, -1, -1, -1, 1, -1, -1, 1, -1, -1, 1, -1, -1, 1, -1, -1, 1, -1, -1, 1, 1, -1, 1, -1
7	1, 1, -1, -1, 1, 1, -1, -1, 1, -1, -1, -1, -1, 1, -1, 1, 1, -1, -1, 1, 1, 1, -1, 1, 1, 1, -1, 1, 1, 1, -1, 1, 1, 1, -1, 1, 1, 1, -1, 1, 1, -1, 1, 1, 1, -1, 1, 1, 1, -1, -1, -1, -1, 1, 1, 1, -1, -1, -1, 1, 1, 1, 1, -1, 1, 1, 1, 1, 1, -1, -1, -1
8	-1, -1 , -1, 1, 1, 1, 1, 1, -1, -1, 1, -1, -1, -1, 1, -1, 1, 1, -1, 1, -1, -1, 1, 1, -1, 1, -1, -1, 1, -1, 1, -1, -1, -1, -1, 1, -1, 1, 1, 1, 1, -1, 1, -1, 1, 1, -1, 1, -1, 1, -1, -1, -1, -1, 1, -1, -1, -1, 1, -1, -1, 1

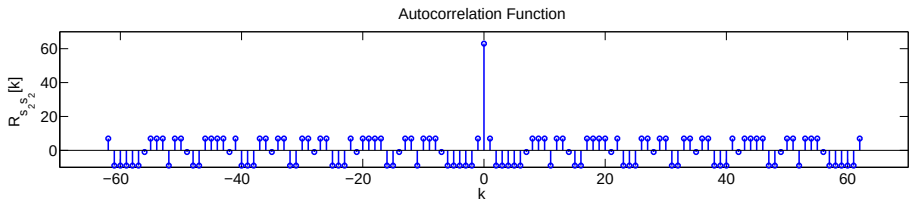

Figure 2.9: Autocorrelation function of one of the generated Kasami sequences

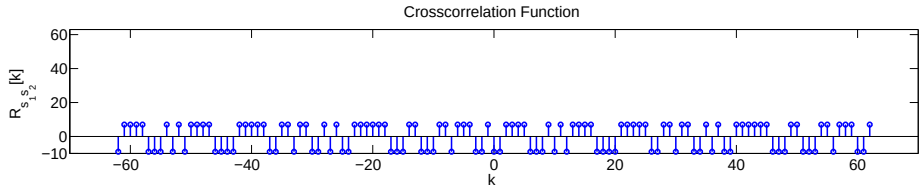

Figure 2.10: Crosscorrelation function of two Kasami sequences

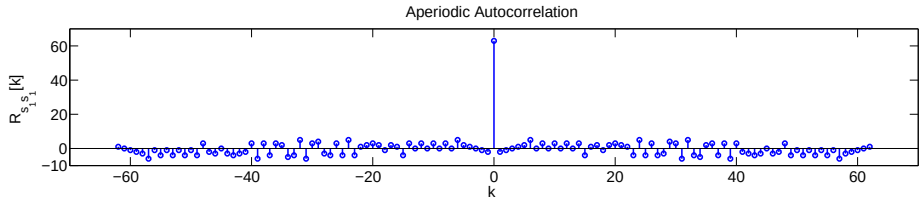

Figure 2.11: Autocorrelation function of aperiodic Kasami sequence

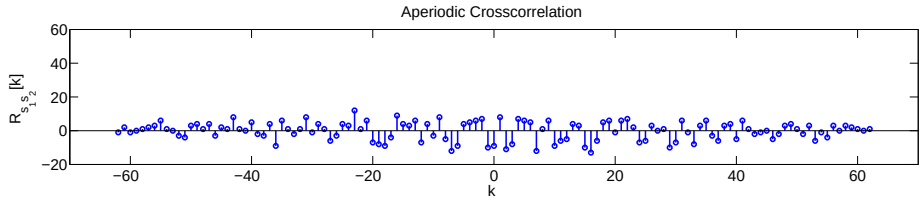

Figure 2.12: Crosscorrelation function of two aperiodic Kasami sequences

2.4.3 Complete System Block Diagram

The general block diagram of the structure used in this thesis is shown in Figure 2.13.

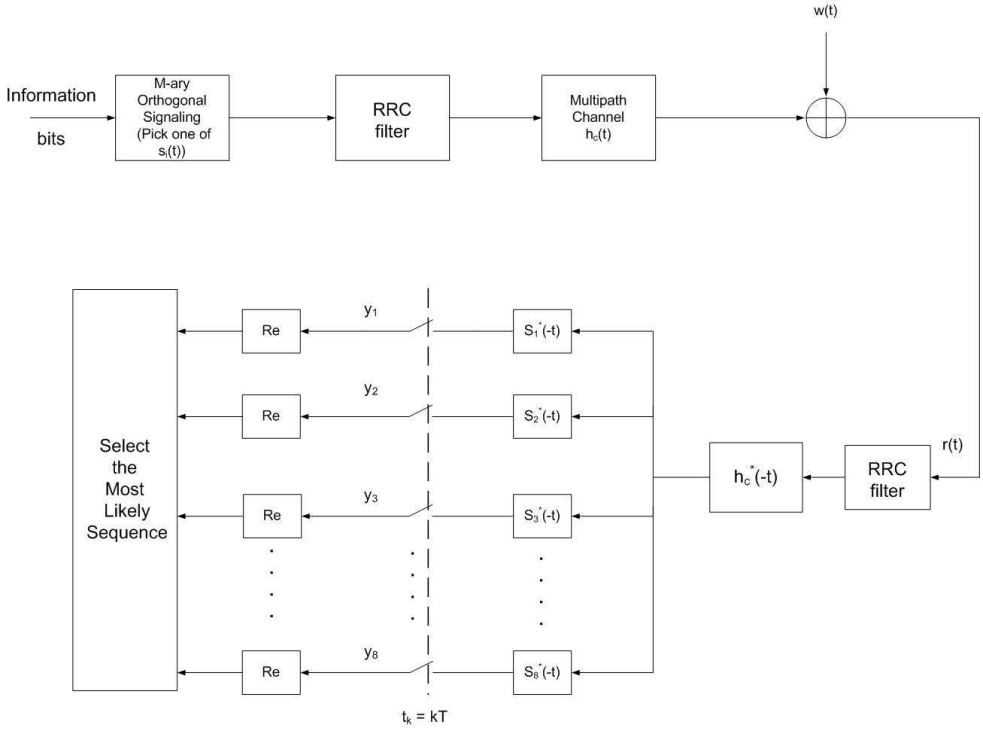

Figure 2.13: Structure used in this work

In order to convey information bits, 8 Kasami sequences with a length $N = 63$ are generated as described in section 2.4.2 and are used as transmitting symbols. At the transmitter, the data is grouped into $k = log_2 M = 3$ bits block. This 3-bit block represents the symbol with a symbol duration T_s which is k times the bit duration T_b. According to each 3-bit block in the input data, a signal waveform is selected from the set of 8 Kasami sequences as the transmitted symbol. Each transmitted symbol consists of $L = 63$ chips and each chip has a duration of T_c:

$$T_s = 3T_b = 63T_c \tag{2.41}$$

The transmitted waveform in baseband is expressed as

$$x(t) = \sum_{k} a_k g(t - kT_c) \tag{2.42}$$

where a_k are chips belonging to the transmitted symbol and $g(t)$ is the pulse shape. We use a Raised Cosine Filter for the overall pulse shaping. Root Raised Cosine Filters (RRC) are used in both the transmitter and the receiver in order to obtain a Raised Cosine Filter as a resultant.

The frame structure of a transmitted packet is shown in 2.14. The training sequence is used for frame synchronization and channel estimation. The information data part consists of 17 symbols (51 bits).

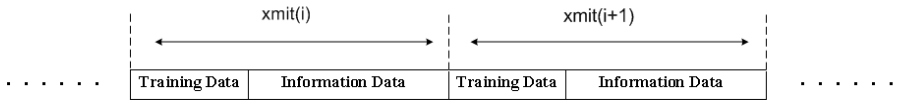

Figure 2.14: Frame structure of a transmitted word

The channel impulse response consisting of L taps is expressed as

$$h_c(t) = \sum_{i=1}^{L} h_i(t)\delta(t - \tau_i) \tag{2.43}$$

where h_i is the complex gain and τ_i is the time delay corresponding to related gain. The channel output is corrupted by white Gaussian noise, $w(t)$.

The receiver is the one already described in section 2.3

In simulations, the packet shown in Figure 2.14 is sent for each transmission burst. In each packet, the information data consists of 17 symbols each of which is represented by one of the generated Kasami sequences. The received signal is obtained by passing the transmitted word through a channel and corrupting it by the white noise. After the demodulation process at the receiver, the detector estimates the transmitted data. Then, the estimated bits and the transmitted bits are compared to detect the number of bit errors in the received data. This process is repeated until the sufficient bit error number is reached.

Moreover, the performance of the proposed structure is explored by simulations carried out in MATLAB. Since simulations are conducted in discrete time, the analog signals involved in the system diagram are sampled at a rate greater than the corresponding Nyquist rate. In most of the simulations, the sampling rate is chosen as 16 times the chip rate:

$$f_{sampling} = \frac{1}{T_{sampling}} = \frac{16}{T_c} \tag{2.44}$$

CHAPTER 3

PERFORMANCE UNDER IDEAL CONDITIONS

3.1 INTRODUCTION

In Chapter 2, M-ary quasi-orthogonal signaling system using Kasami codes has been proposed. Kasami codes are not orthogonal but they take low cross-correlation values. Hence they can be treated as nearly orthogonal signals. In this chapter, the performance of M-ary Kasami code signaling is explored by using the proposed receiver structure under AWGN channel. Moreover, Kasami codes are used in an M-ary biorthogonal structure by including negatives of Kasami codes as a transmitted symbol. Then, the performance of this structure is observed and compared with the M-ary Kasami codes signaling.

3.2 IDEAL M-ARY ORTHOGONAL SIGNALING

In order to explore the performance of our proposed M-ary signaling system using quasi orthogonal codes, it is needed to compare our simulation results with the exact M-ary orthogonal modulation under ideal conditions. In Chapter 2, details of M-ary orthogonal signaling are described. As mentioned in Chapter 2, for M equal-energy orthogonal signals the symbol error probability is

$$P_M = \frac{1}{\sqrt{2\pi}} \int_{-\infty}^{\infty} \left[1 - \left(\frac{1}{\sqrt{2\pi}} \int_{-\infty}^{y} e^{-x^2/2} dx \right)^{M-1} \right] exp \left[\frac{-1}{2} \left(y - \sqrt{\frac{2\epsilon}{N_0}} \right)^2 \right] dy \qquad (3.1)$$

The bit error probability can be derived from the symbol error probability. Each symbol conveys k bits of information where $k = log_2 M$ and the average number of n bit errors per k-bit symbol is expressed as follows:

$$E\{\text{n bit errors}\} = \sum_{n=1}^{k} \binom{k}{n} \frac{P_M}{2^k - 1} = k \frac{2^{k-1}}{2^k - 1} P_M \tag{3.2}$$

Then the bit error probability is

$$P_b = \frac{2^{k-1}}{2^k - 1} P_M \approx \frac{P_M}{2} \qquad k >> 1 \tag{3.3}$$

The graphs of the bit error rate as a function of SNR per bit, ε_b/N_0 are shown in Figure 3.1 for $M = 2, 4, 8, 16, 32$.

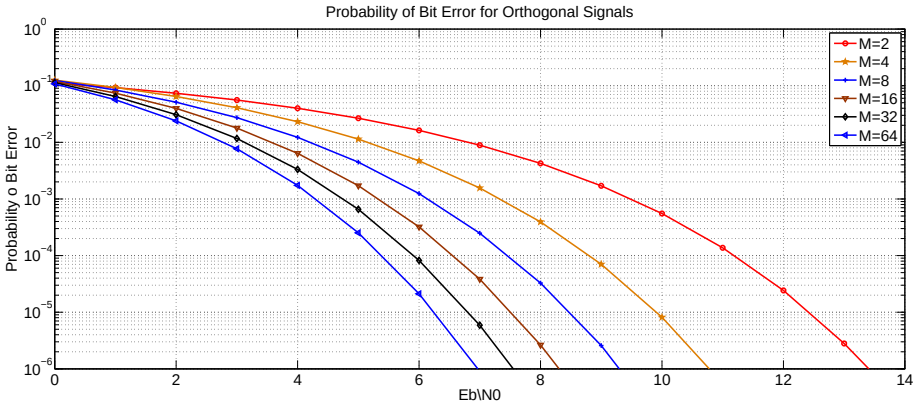

Figure 3.1: Probability of bit error of M-ary orthogonal signals for different M values

3.2.1 Simulations and Comparisons

First, the performance of the proposed M-ary signaling structure using Kasami codes is investigated. For this purpose, Monte-Carlo simulations have been carried out for the AWGN channel assuming perfect synchronization. The exact M-ary orthogonal signaling, the formula of which is given in equation (3.1), can be used as a reference to compare our simulation result. The number of Kasami codes used in our proposed system is $M = 8$ with or $N = 63$ chips. Figure 3.2 shows the performance of M-ary Kasami codes signaling.

As seen in Figure 3.2, the performance of the proposed system using Kasami codes is better than M-ary orthogonal modulation. This performance improvement is attributed to the cross

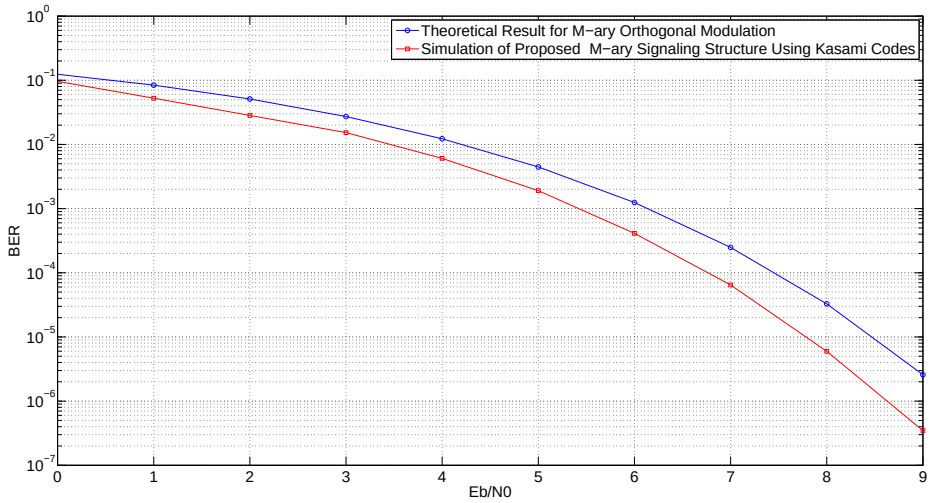

Figure 3.2: Performance of M-ary signaling system using Kasami codes

correlation property of Kasami sequences: Since the correlation of any two Kasami sequences can take negative values, the distance between symbols is increased.

3.3 M-ARY BIORTHOGONAL SIGNALING

M-ary biorthogonal signaling which is deduced from M-ary orthogonal signaling can be used in digital communication systems. A set of M biorthogonal signals can be constructed from $M/2$ orthogonal signals by including negatives of orthogonal signals [2]. Hence in order to construct a set of M biorthogonal signals $N = M/2$ dimensions are required. Signal space diagrams for some biorthogonal signals are shown in Figure 3.3.

The complexity of the receiver is reduced for biorthogonal signaling, since in M-ary biorthogonal signaling the receiver is implemented with $M/2$ correlators or matched filters while in orthogonal signaling M correlators are required. In [2] an expression for the probability of correct decision of M-ary biorthogonal signaling is derived:

$$P_c = \int_{-\sqrt{2\epsilon_s/N_0}}^{\infty} \left(\frac{1}{\sqrt{2\pi}} \int_{-(v+\sqrt{2\epsilon_s/N_0})}^{(v+\sqrt{2\epsilon_s/N_0})} e^{-x^2/2} dx \right)^{M/2-1} e^{-v^2/2} dv \tag{3.4}$$

The symbol error probability for M-ary biorthogonal signals is then found as

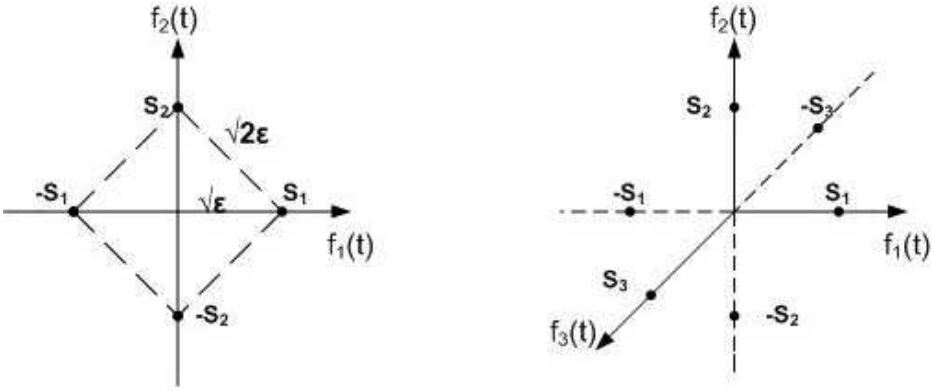

Figure 3.3: Signal space diagrams of biorthogonal signals for M=4, N=2 and M=6, N=3

$$P_M = 1 - P_c \tag{3.5}$$

Figure 3.4 illustrates the symbol error rate as a function of SNR per bit for different values of M.

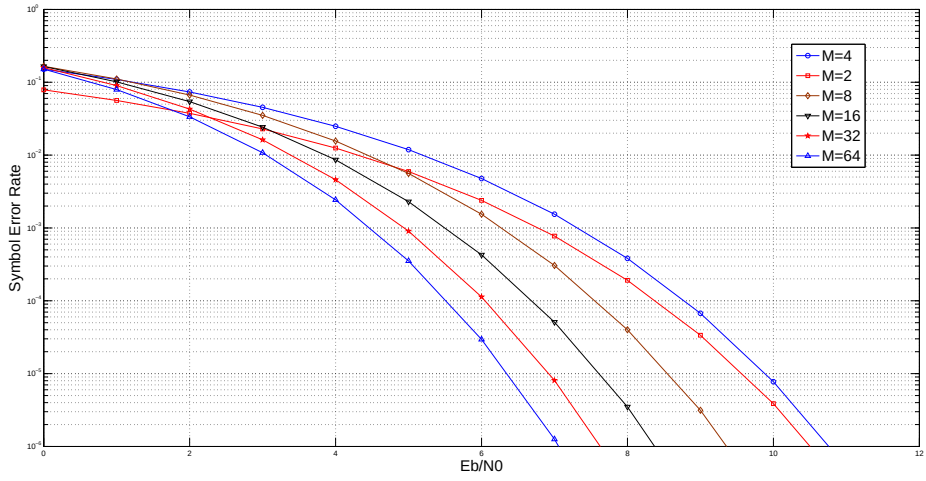

Figure 3.4: Probability of symbol error for biorthogonal signals

3.3.1 Simulations and Comparisons

In this section we investigate the performance of Kasami codes in biorthogonal structure. We have totally 16 sequences with length $N = 63$ to transmit information by considering negatives of 8 generated Kasami sequences. For $M = 16$, $log_2 M = 4$ bits are conveyed by each sequence. In contrast, in M-ary orthogonal signaling using Kasami codes 3 bits are conveyed by each sequence. In order to see the performance of M-ary biorthogonal signaling using Kasami codes, the same structure for M-ary orthogonal signaling shown in Figure 2.13 is used. Again, in the demodulator part, real parts of the symbol matched filter outputs are used for decision. Symbol matched filters are matched to 8 Kasami sequences. At the receiver, the detector first selects the related matched filter by picking up the maximum of the absolute value of matched filter outputs. Then the transmitted symbol is determined by looking for the sign of the selected symbol matched filter output. The implementation of the receiver is similar to the structure used for M-ary orthogonal signaling. The only difference between these receiver structures is that the absolute value of matched filter outputs in M-ary biorthogonal signaling are used instead of themselves. Hence the advantage of having negative cross-correlation value between the Kasami codes is lost.

The performance of M-ary biorthogonal signals for $M = 16$ is illustrated in Figure 3.5. The theoretical result given in Figure 3.4 is used as a reference to compare the performance of M-ary biorthogonal modulation using Kasami codes.

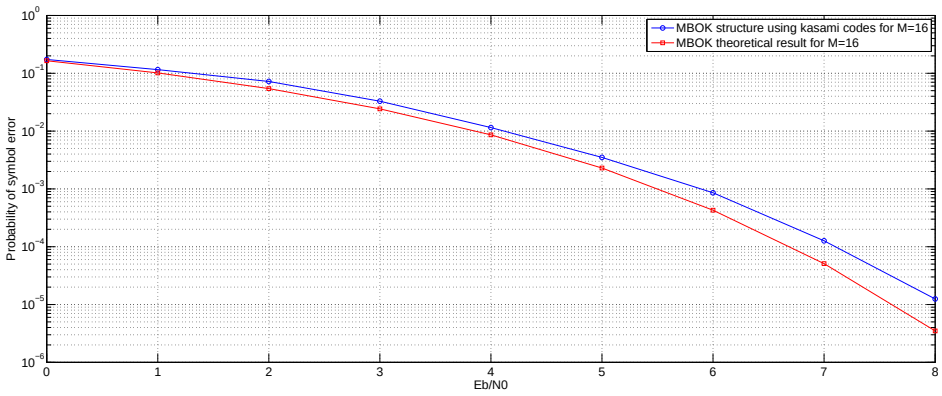

Figure 3.5: Performance of M-ary biorthogonal structure using Kasami codes

It is seen in Figure 3.5 that the performance of biorthogonal signaling using Kasami codes is worse than the biorthogonal signaling using orthogonal signals as expected.

We also compare the performance of M-ary biorthogonal signaling using Kasami codes with M-ary Kasami code signaling. For this comparison, we equate the dimensions of both modulations to 8. The number of sequences is:

$$M_{orth} = 8 \qquad M_{borth} = 16$$

The performance comparison for these signaling schemes can be made by examining Figure 3.6.

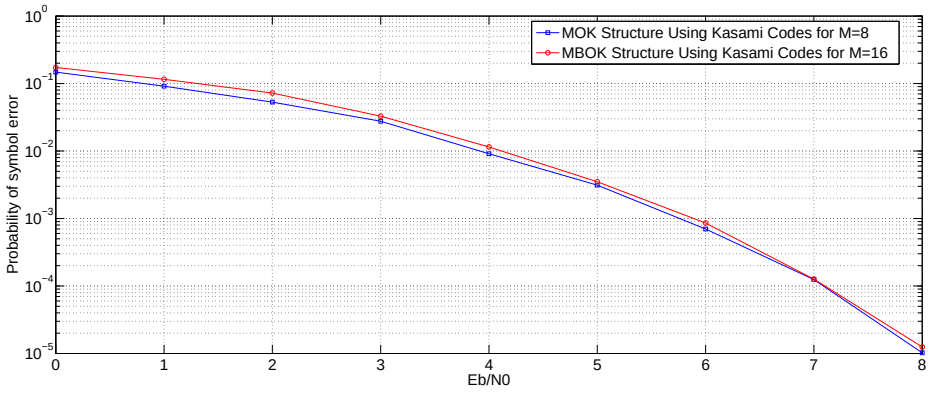

Figure 3.6: Comparison of M-ary signaling and M-ary biorthogonal structure using Kasami codes

As seen in Figure 3.6, performances of these systems are very close to each other. One of the advantages of M-ary biorthogonal signaling is that higher data transmission rate is achieved which means higher spectral efficiency. In an equal symbol time interval, the number of bits conveyed by a Kasami symbol is

$$\begin{aligned} log_2 M_{orth} &= 3 \qquad \text{for M-ary orthogonal structure} \\ log_2 M_{borth} &= 4 \qquad \text{for M-ary biorthogonal structure} \end{aligned} \tag{3.6}$$

Hence, in M-ary biorthogonal signaling, more bits can be transmitted in a symbol. This allows us to use error correction codes in M-ary biorthogonal signaling with the same information bit

rate as the uncoded M-ary orthogonal signaling. Therefore, the performance can be improved by M-ary biorthogonal signaling.

CHAPTER 4

A SIMPLE SYMBOL SYNCHRONIZER

4.1 INTRODUCTION

In communication systems, the parameters required by most receivers are the carrier frequency, the carrier phase and the symbol timing of the received signal [18]. The carrier frequency of the received signal may be different from that of the nominal value of the transmitter carrier frequency. This discrepancy could be due to the deviation of the transmitter oscillator and the receiver oscillator from the nominal frequency and the Doppler effect. In reality, the information-bearing signal travels from the transmitter to the receiver within a finite amount of time. This transmission delay introduces a mismatch between the symbol timing at the transmitter and that at the receiver. The matched filter output needs to be sampled at an exact time in order to optimize the receiver performance. The carrier phase of the received signal is the sum of three major components, namely, the random phase due to the mismatch between the local oscillators of the transmitter and the receiver, the channel phase response and the phase stemming from the transmission delay. In this chapter, we focus on estimation of symbol timing. Since the prorogation delay from the transmitter to the receiver is unknown at the receiver, the symbol timing must be derived from the received signal in order to sample the demodulator output synchronously. The process of extracting the clock for determining the accurate location of the symbol timing at the receiver is called symbol synchronization or symbol timing recovery [2]. A system that is able to estimate such locations is called a timing (or) clock synchronizer.

Suppose the channel delays the signal transmitted through it and corrupts the signal by adding

Gaussian noise. Hence, the received signal is

$$r(t) = s(t - \tau) + w(t) \tag{4.1}$$

where τ is the propagation delay and $w(t)$ is the white Gaussian noise with two-sided spectral density $N_0/2$. The transmitted signal $s(t)$ in equation 4.1 is given by

$$s(t) = \sum_k a_k g(t - kT) \tag{4.2}$$

where a_k are data symbols belonging to the M-ary alphabet and g(t) is the pulse shape with a time interval T. In general, the typical block diagram of a baseband receiver with a symbol synchronizer is indicated in Figure 4.1.

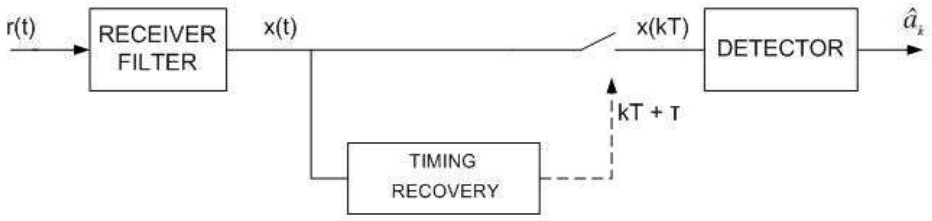

Figure 4.1: Block diagram of a baseband receiver

After the incoming waveform is filtered in order to remove the out-of-band noise, the output of the filter is sampled periodically at T-spaced instants, that is $t = kT + \hat{\tau}$. Via these samples, the detector derives estimates $\hat{a_k}$ of the transmitted data. The timing recovery function aims at generating optimum sampling instants which amount to the maximum eye opening at the output of the receiver filter [11]. Hence, by using these estimated samples the receiver achieves a bit error rate as close as possible to optimum.

Mengali and D' Andrea in [11] state two topologies used for the symbol synchronization in digital communication systems, i.e. feedback(closed loop) configuration and feedforward (open loop) configuration. Figures 4.2 and 4.3 illustrate configurations pertaining to these topologies. In both cases, the received signal applies to AAF (Anti-Aliasing Filter) which limits the bandwidth of the received signal. Sampling is controlled by a fixed clock whose ticks are not locked to the incoming data. The bulk of the pulse shaping is performed in the

matched filter whose location is not necessarily that shown in the figures. Timing correction is similar to the operation of a voltage controllable delay line and produces synchronized samples to be used for decision and synchronization purposes [11].

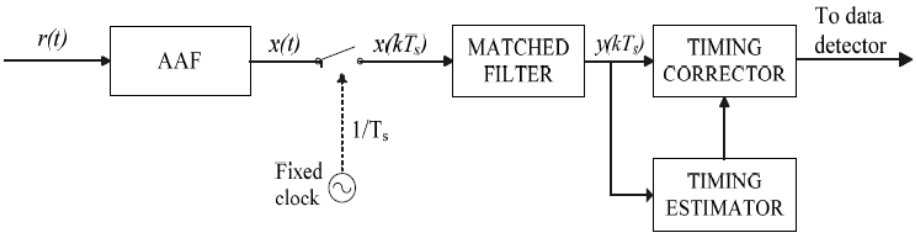

Figure 4.2: Feedforward configuration

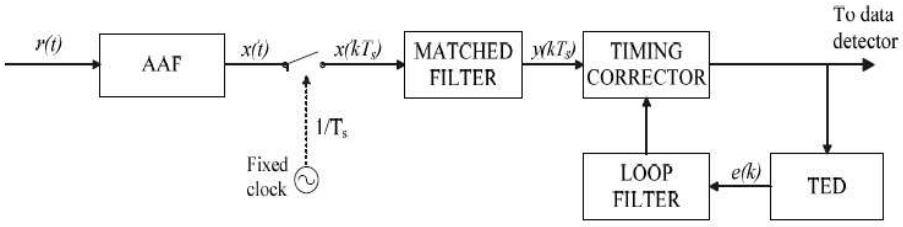

Figure 4.3: Feedback configuration

In feedforward configuration, an estimate of the timing information is derived by processing received signal samples. Whereas, in feedback configuration a timing corrector feeds a timing error detector (TED) the purpose of which is to generate an error signal $e(k)$ in proportion to the difference between the prorogation delay τ and its current estimate. Symbol synchronization methods can be classified into two groups: Decision directed methods and non-decision directed methods.

In this chapter, a new symbol timing synchronizer suitable for M-ary signaling is proposed and the performance of this synchronizer is explored.

4.2 PROPOSED SYMBOL SYNCHRONIZATION

In this work, a non-decision directed timing recovery scheme is proposed in order to derive symbol timing information. The proposed timing synchronizer has its roots from the Maximum Likelihood (ML) estimation of the timing offset. The likelihood function is given by

$$\Lambda(\hat{\tau}) = C_L \int_{T_0} r(t)s(t-\hat{\tau})dt \tag{4.3}$$

for estimating the time of arrival of known signal s(t) in AWGN. Thus, the likelihood function is just a correlation process. The most likely timing offset t_{offset} is the value of $\hat{\tau}$ which maximizes the likelihood function:

$$\hat{t}_{offset} = \underset{\hat{\tau}}{\text{argmax}}\Lambda(\hat{\tau}) \tag{4.4}$$

For M-ary signaling, each $log_2 M$ bit block is conveyed by one of M specific waveforms. Suppose the transmitted signal is delayed by the channel and corrupted by Gaussian noise. Hence, the received signal is given by

$$y(t) = \sum_{k=0}^{K} s_{I_k}(t - kT_s - \tau) + w(t) \tag{4.5}$$

where I_k represents one of M symbols. The sequentially transmitted symbols are denoted by $\underline{\mathbf{I}}$ vector:

$$\underline{\mathbf{I}} = \{I_1, I_2, \ldots, I_K\} \tag{4.6}$$

In our proposed timing recovery, the timing offset τ is estimated by maximizing the probability density function $p(\underline{y}|\tau, I)$ with respect to unknown signal parameters τ and I as follows:

$$\{\hat{\underline{\mathbf{I}}}, \hat{\tau}\} = \underset{\tau,I}{\text{argmax}}\, p(\underline{y}|\tau, I) \tag{4.7}$$

$$\{\hat{\underline{\mathbf{I}}}, \hat{\tau}\} = \underset{\tau,I}{\text{argmax}} \sum_{k=0}^{K} \int_{kT_s}^{(k+1)T_s} y(t)s_{I_k}(t - kT_s - \tau)dt \tag{4.8}$$

$$\{\hat{\underline{\mathbf{I}}}, \hat{\tau}\} = \underset{\tau, I}{\operatorname{argmax}} \sum_{k=0}^{K} y^{I_k, \tau} \tag{4.9}$$

where $y^{I_k,\tau}$ is the matched filter output of k-th symbol with a certain time delay τ. The symbol timing offset may be estimated by looking for the timing instant where the maximum of the correlation between the received signal and reference signals is obtained. This is the optimal decoding method. However, this method is rather complex. Since there are M matched filters, the process in equation 4.8 is repeated M^K times in order to estimate the timing offset. One can simplify this optimal decoding by using suboptimal symbol by symbol decision:

$$\{\hat{\tau}\} = \underset{\tau}{\operatorname{argmax}} \sum_{k=0}^{K} \underset{I_k}{\operatorname{max}} y^{I_k, \tau} \tag{4.10}$$

In this suboptimal decoding, the complexity to make symbol decision reduces since the process in equation 4.10 is repeated $M \cdot K$ times. This correlation function may also be evaluated as the output of a filter matched to the reference signal. For M-ary signaling, we use M filters each of which is matched to one of the possible M signals. After the received samples are passed through the matched filters each of which matched to a signal in the set, $s_i(t)$, the matched filter outputs resemble those shown in Figure 4.4.

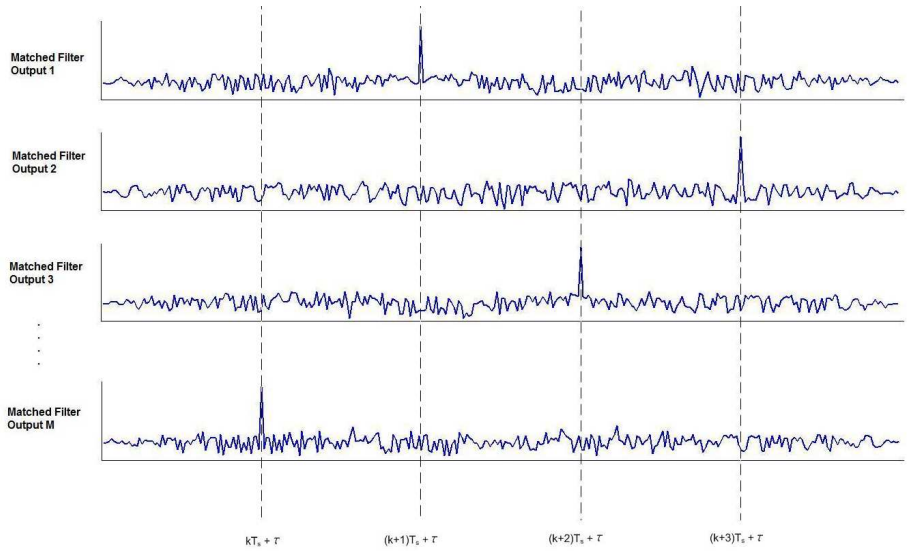

Figure 4.4: Matched filter outputs

As seen in the matched filter outputs, different matched filter outputs give maximum correlation values at T_s-spaced instants with a propagation delay τ. For the estimation of the timing offset as expressed in equation 4.10, we construct a function which is called "comb" function. The "comb" function comprises a kind of time-gate function which has a periodic structure and a certain time offset as shown in Figure 4.5.

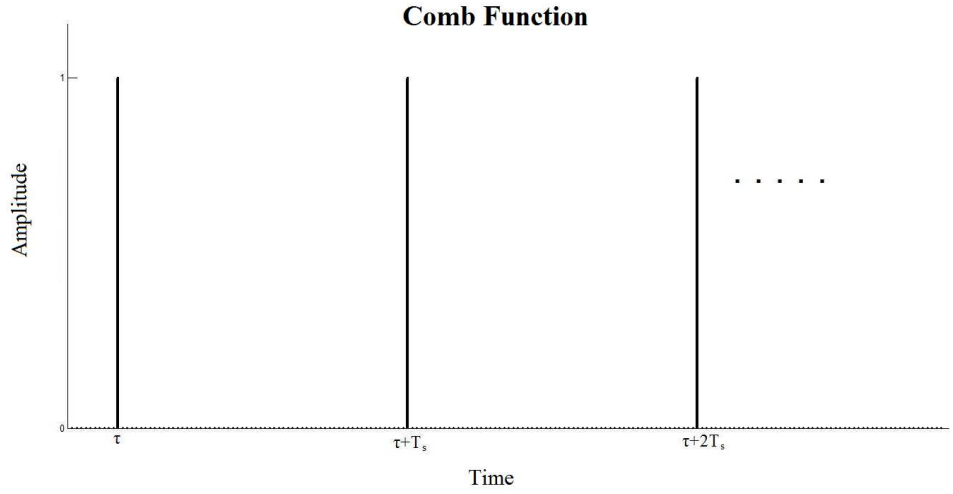

Figure 4.5: "Comb" Function

The "comb" function is used to look for the timing instant where we obtain the maximum value at the channel matched filter outputs. For this purpose, the "comb" function is applied to matched filter outputs to sample the matched filter outputs at the time $\tau + kT_s$. Functionally, at time instances $\tau + kT_s$ all matched filter outputs are sampled, the one with maximum value at $\tau + kT_s$ is chosen and all these maximum values are added to get the function's value at the time delay τ. This process is repeated for all $0 \leq \tau < T_s$. Finally, the value τ for which the "comb" function is maximum is declared the estimated time offset. This timing offset estimation process is shown in Figure 4.6.

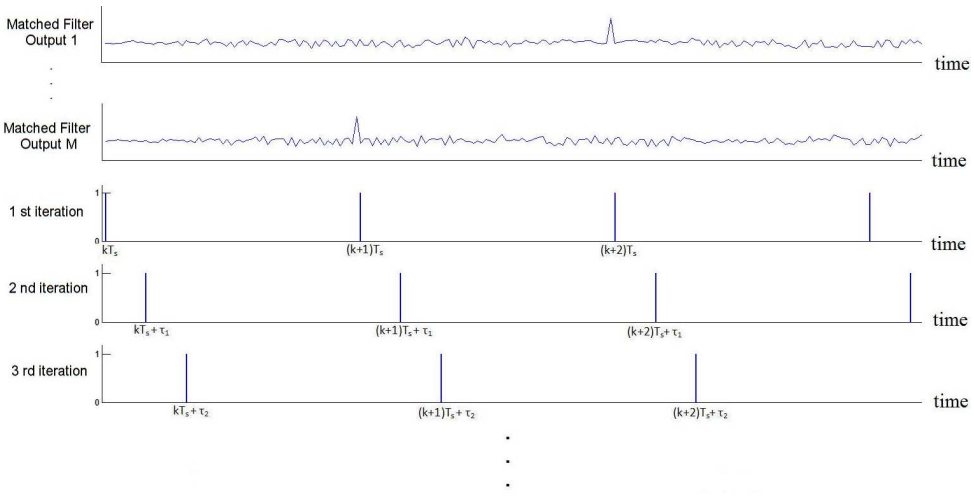

Figure 4.6: Timing recovery process: In each iteration, the "comb" function is shifted in time by a certain time offset τ and all matched filter outputs are sampled at $t = \tau + kT_s$. After choosing the sample with maximum value at $t = \tau + kT_s$, these maximum values are added. After completing all iterations, the sum values obtained in each iteration are compared and the largest sum value is chosen. The value τ where the "comb" function is maximum is the estimated time offset.

In the following part of this section, in order to apply the proposed timing recovery the written matlab code is given:

%matched filter outputs are combined in a function by selecting the maximum valued sample between the samples of all matched filter outputs.

```
for i=1:length(r1)
    w1(i)=max(r1(i),r2(i));
    w2(i)=max(w1(i),r3(i));
    w3(i)=max(w2(i),r4(i));
    w4(i)=max(w3(i),r5(i));
    w5(i)=max(w4(i),r6(i));
    w6(i)=max(w5(i),r7(i));
    s(i)=max(w6(i),r8(i));
end
```

%create the "comb" function which is equal to 1 at $t = mT_s$ *where* $m = 0, 1, 2 \ldots$, *total symbol number*-1.

```
combfunc=zeros(1,16*length(k1)+1);
for z=1:1:17
    combfunc((z-1)*length(k1)+1)=1; % length(k1)=symbol time
end
```

%multiply the terms of s[k] by the terms of a time shifted combfunc[k] and add them up. All sum values are compared and the symbol timing offset is estimated by picking up the time shift with the largest sum value.

```
for i=1:1:length(k1)*2-1)
    a=s(i:1:(i+16*length(k1))) .* combfunc;
    b(i)=sum(a);
end
[maxnumber,sampletime]=max(b);
```

4.3 MODIFIED CRAMER-RAO BOUND [11][12]

Cramer-Rao Bound (CRB) is a useful tool which gives a lower bound on the error variance of any parameter estimator [13].

Suppose that the complex envelope of the received signal is given by

$$r(t) = s(t) + w(t) \tag{4.11}$$

where

$$s(t) = exp\, j[2\pi v(t - t_0) + \theta] \sum_k a_i g(t - kT - \tau) \tag{4.12}$$

and w(t) is the complex valued additive white Gaussian noise. In 4.12, v is the carrier frequency offset, θ is the carrier phase at some reference time $t = t_0$ and τ is the symbol time delay. These three parameters v, θ, τ are unknown and should therefore be estimated at the receiver. In this work, we focus on estimating the symbol timing offset τ. CRB defines a bound for a variance of any parameter estimation error. Let a single element of v, θ, τ be denoted

by λ which is assumed to be deterministic (nonrandom). All other parameters and the data are gathered in a vector $\mathbf{u}$ having a known probability density function $p(\mathbf{u})$. If $\hat{\lambda}(\mathbf{r})$ is any unbiased estimate of λ, then the CRB is given by

$$Var\left[\lambda - \hat{\lambda}(\mathbf{r})\right] \geq CRB(\lambda) = \frac{1}{E_{\mathbf{r}}\left\{\left[\frac{\partial p(\mathbf{r}|\lambda)}{\partial \lambda}\right]^2\right\}} \tag{4.13}$$

or equivalently,

$$CRB(\lambda) = -\frac{1}{E_{\mathbf{r}}\left\{\left[\frac{\partial^2 p(\mathbf{r}|\lambda)}{\partial^2 \lambda}\right]\right\}}. \tag{4.14}$$

The Cramer-Rao Bound expression given in equations (4.13) and (4.14) provides a bound for the variance of the estimation error. It is known that no unbiased estimator can provide a lower variance than that established by CRB. Although this bound provides a lower limit for the estimation error, the computation of $p(\mathbf{r}|\lambda)$ contains some mathematical difficulties. The probability density function $p(\mathbf{r}|\lambda)$ is derived by averaging out the unwanted parameters from $p(\mathbf{r}|\mathbf{u}, \lambda)$:

$$p(\mathbf{r}|\lambda) = \int_{-\infty}^{\infty} p(\mathbf{r}|\mathbf{u}, \lambda) p(\mathbf{u}) d\mathbf{u} \tag{4.15}$$

Unfortunately, in most cases of practical interest, the computation of the CRB formula is difficult since either the integration in equation 4.15 cannot be carried out analytically or there are obstacles risen in calculating the expectation in equation 4.14 [12]. Another lower bound to the variance of the estimation error is the Modified Cramer-Rao Bound (MCRB) [11] [12]. MCRB is much easier to employ but it is generally looser than CRB.

MCRB is a variant of CRB and it is derived by using Jensen's inequality in the CRB formula. MCRB by [12] for the variance of $\lambda - \hat{\lambda}(\mathbf{r})$ is as follows

$$MCRB(\lambda) = \frac{1}{E_{\mathbf{r},\mathbf{u}}\left\{\left[\frac{\partial ln p(\mathbf{r}|u, \lambda)}{\partial \lambda}\right]^2\right\}}, \tag{4.16}$$

where u represents a set of nuisance parameters.

The relationship between $CRB(\lambda)$ and $MCRB(\lambda)$ is

$$Var\left[\lambda - \hat{\lambda}(\mathbf{r})\right] \geq CRB(\lambda) \geq MCRB(\lambda) \tag{4.17}$$

In Figure 4.7, examples of $CRB(\lambda)$ and $MCRB(\lambda)$ are drawn as a function of the signal to noise ratio E_s/N_0 in case MCRB is looser, i.e. too low in comparison to the error variances of good estimators. MCRB and CRB become identical when unwanted parameters in **u** are perfectly known or there are no unknown parameters.

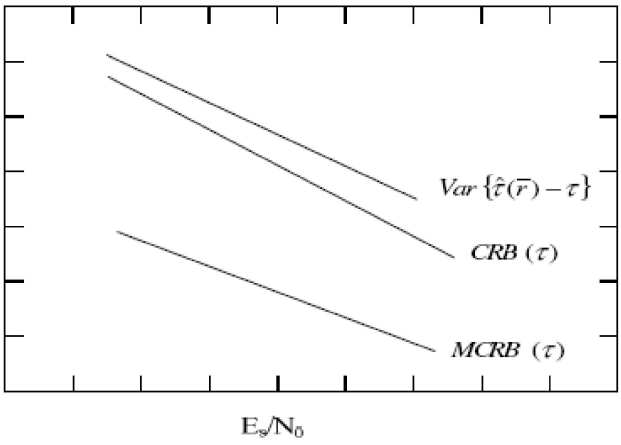

Figure 4.7: Example curves: Actual error variance, CRB(λ), MCRB(λ) [11]

In this study, we consider the estimation of the symbol timing delay τ. In order to compute MCRB for the separate estimation of $\{\tau, \theta, v\}$ following assumptions are made: While deriving $MCRB(\lambda)$, λ is considered as a fixed parameter and the vector u including unwanted parameters and data symbols $\{a_i\}$ is considered as a random vector. Suppose $\lambda = v$. In computing $MCRB(v)$, we consider v as a fixed parameter and $u_v = \{\tau, \theta, a_i\}$ as a random vector. Similar assumptions are made for $\lambda = \tau$, $\lambda = \theta$ and their associated unwanted parameter vectors $u_\tau = \{v, \theta, a_i\}$ and $u_\theta = \{\tau, v, a_i\}$. In addition, there are some assumptions made on statistics of parameters $\{\tau, \theta, v, a_i\}$. It is assumed that the timing epoch τ in u_v and u_θ is uniformly distributed between 0 and symbol interval T. Data symbols a_i are zero mean independent random variables. Finally, synchronization parameters included in any of the vectors u_v, u_τ,

u_θ are independent.

In this thesis, only the estimation of timing delay τ is considered. In [12], the MCRB for τ is given by

$$MCRB(\tau) = \frac{B_L T}{4\pi^2 \xi} \frac{T^2}{E_s/N_0} \tag{4.18}$$

where ξ is a coefficient depending on the pulse shape $g(t)$:

$$\xi \cong \frac{\int_{-\infty}^{\infty} T^2 f^2 |G(f)|^2 \, df}{\int_{-\infty}^{\infty} |G(f)|^2 \, df} \tag{4.19}$$

In equation 4.18, the equivalent noise bandwidth B_L is:

$$B_L = \frac{1}{2LT} \tag{4.20}$$

where LT equals the observation time interval T_0.

The bound in equation 4.18 will be used as a reference in performance comparisons in the sequel.

4.4 SIMULATIONS AND RESULTS

In this section, the performance of the proposed synchronizer is investigated under AWGN channel. For simulation of the proposed synchronizer, a model is developed in MATLAB. Hence, continuous time signals must be represented by their discrete time samples taken at a rate greater than the Nyquist rate in the simulation model. In simulations, the discrete time samples are taken at a rate $f_{sampling} = 1/T_{sampling}$ where

$$T_{sampling} = \frac{T_c}{16}$$

where T_c represents the chip time interval. Transmitted symbols consist of chips belonging to the relevant Kasami code. The block diagram of the simulated model is shown in Figure 4.8.

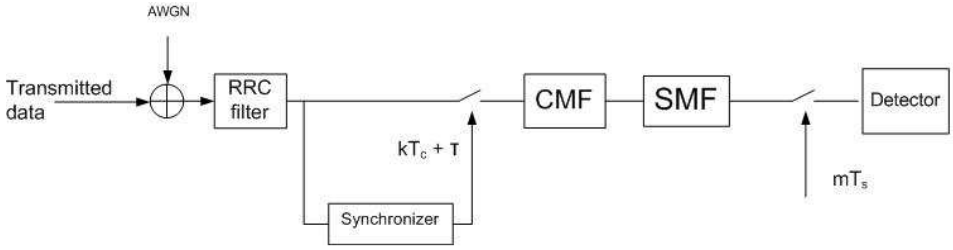

Figure 4.8: Simulated model of a receiver

The received signal is

$$x(t) = \sum c_n g(t - nT_c) + w(t) \tag{4.21}$$

where $g(t)$ denotes the pulse shape and $w(t)$ represents the white Gaussian noise. The proposed symbol synchronizer produces the estimate of the sampling time:

$$t_k = kT_c + \hat{\tau} \tag{4.22}$$

where $\hat{\tau}$ is the estimate of the symbol timing offset. Having sampled the received signal at the sampling instant produced by the timing synchronizer, the signal becomes

$$x_k = \sum c_n g(kT_c + \hat{\tau} - nT_c) + w(kT_c + \hat{\tau}) \tag{4.23}$$

Then, the receiving process continues in the manner as described in Chapter 2. Initially, the receiver model without synchronizer is considered in order to investigate the receiver delay sensitivity. For this purpose, the received signal is sampled at the exact sampling time with a known fractional delay as follows:

$$t_k = kT_c + \tau_{exact} + m\frac{T_c}{16} \quad \text{where } m = 1, 2, \ldots, 16 \tag{4.24}$$

For each factional delay, the bit error performance is observed. Simulations that are carried out for SNR=4 dB and SNR=6 dB are illustrated in Figures 4.9 and 4.10.

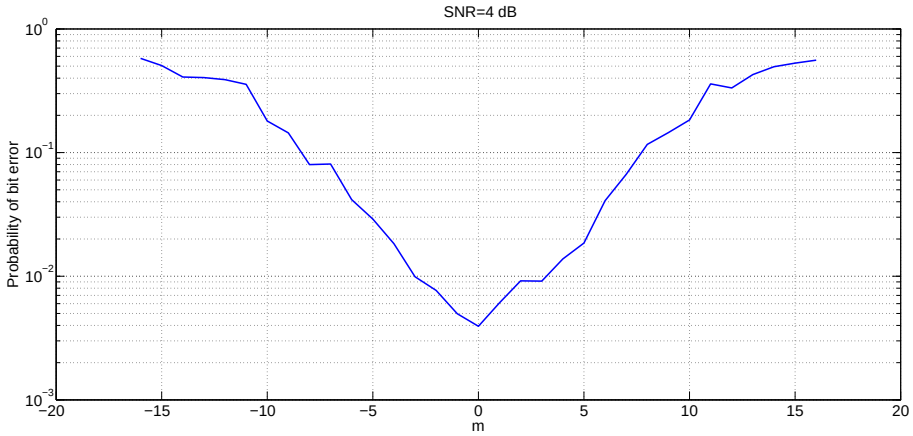

Figure 4.9: Receiver delay sensitivity for SNR=4 dB

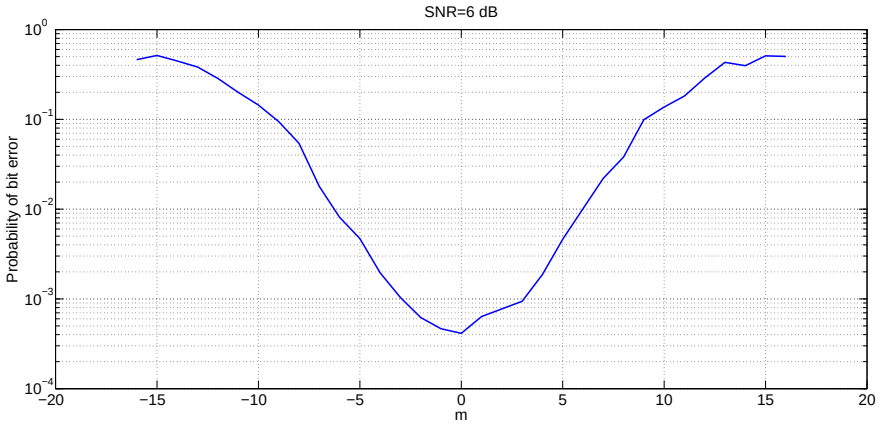

Figure 4.10: Receiver delay sensitivity for SNR=6 dB

As seen in these figures, the receiver performance is degraded when the offset to the exact sampling time is increased.

Furthermore, the receiver sensitivity to the symbol timing delay is explored under a multipath environment. Hilly Terrain channel model is used as an example (The details of this channel model will be given in the next chapter). The simulation is carried out for the chip duration $T_c = 0.1\ \mu sec$ and SNR=6 dB. Also, it is assumed that the channel is known at the receiver. In order to see the receiver timing delay sensitivity in a presence of multipath channel, the received signal is sampled at the exact sampling time with a known fractional delay as shown in equation 4.24. According to the simulation result shown in Figure 4.11, it is illustrated that

the receiver is less sensitive to the symbol timing in a multipath environment when compared to the condition where the channel is AWGN.

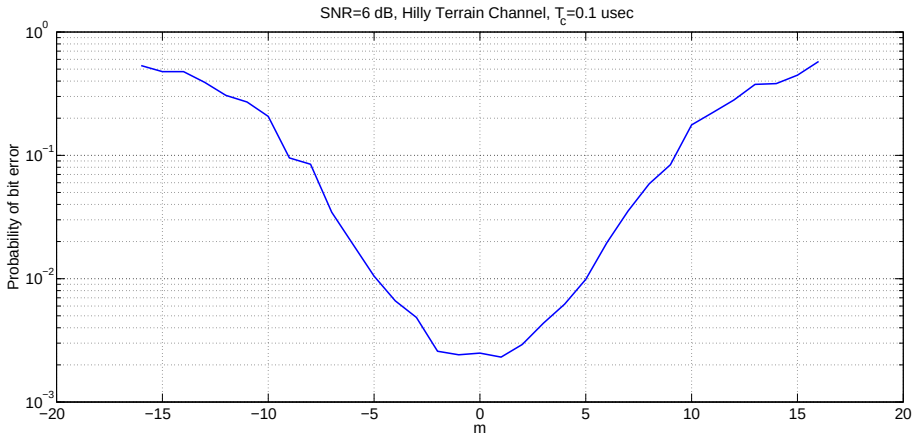

Figure 4.11: Receiver delay sensitivity under a multipath environment for SNR=6 dB

Later, performance of the proposed synchronizer is tested. For this purpose, the BER performance of M-ary Kasami code signaling with the symbol synchronizer is tested and the simulation result is presented in Figure 4.12.

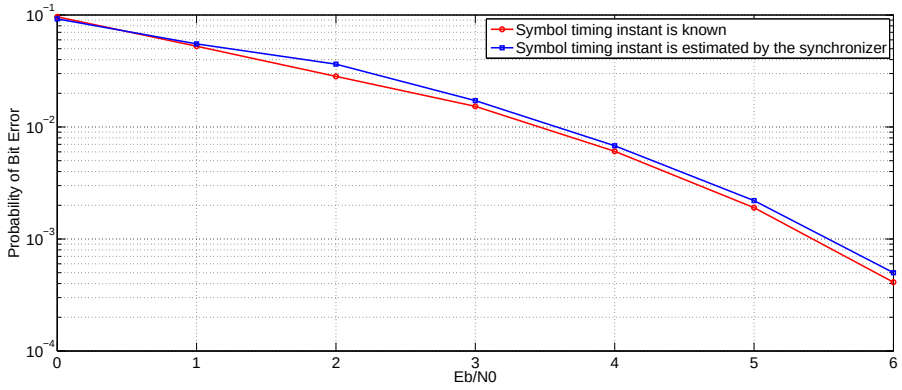

Figure 4.12: BER performance with synchronizer

In addition to the BER performance, the synchronizer performance is tested by considering the symbol timing error (also called jitter). The symbol timing error is:

$$error = \text{exact sampling time-estimated sampling time} = \tau - \hat{\tau}$$

MCRB is used as a reference to test the proposed synchronizer. The MCRB formula for the symbol timing τ is given by

$$\frac{1}{T^2} \times MCRB(\tau) = \frac{1}{8\pi^2 L\xi} \frac{1}{E_s/N_0} \tag{4.25}$$

where L is the number of observed symbols during the timing offset estimation process. Since in each transmission burst 17 symbols are sent, the observed symbol number to estimate the timing offset is 17. In Figure 4.13, the standard deviation of the timing estimation error is compared with the MCRB for the estimate of the timing error.

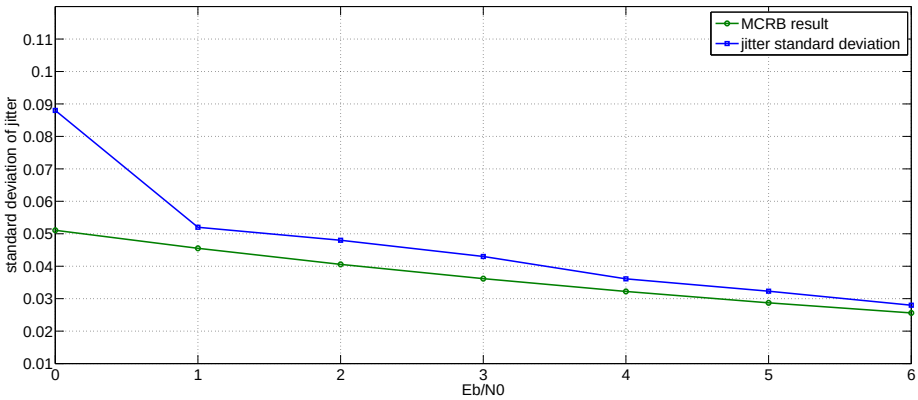

Figure 4.13: Synchronizer timing error standard deviation

It is seen in Figure 4.12 that the BER performance of the system with the symbol synchronizer is very close to the performance with perfect synchronization: There is approximately a 0.1 dB loss due to the proposed symbol timing recovery structure. Considering Figure 4.13 we can conclude that the performance of the synchronizer is somewhat worse than the MCRB. However the difference diminishes as the SNR increases.

CHAPTER 5

CHANNEL ESTIMATION

5.1 INTRODUCTION

Multipath fading is one of the major concerns in wireless communications. A multipath transmission takes place when a transmitted signal arrives at a receiver via two or more paths with different delays. Such multiple paths may be due to the atmospheric reflection or refraction, or reflections from buildings or other objects [15]. Each path can have a separate phase, attenuation, delay and Doppler shift associated with it. Some adverse effects of multipath propagation are inter symbol interference (ISI) and signal fading. These effects significantly limit the performance of a wireless communication system. A RAKE receiver can be used in order to mitigate multipath channel effects. It is described in Chapter 2 that the channel matched filter (CMF) is utilized in our proposed receiver structure for processing the incoming signal and the channel matched filter provides a RAKE receiver implementation. Obviously, the channel matched filter needs to know the channel. This is accomplished by estimating channel parameters. Then, the receiver uses the estimate of the channel in order to detect the transmitted information from the received signal. In general, channel estimation methods can be classified into two groups:

- **Data Aided Channel Estimation:** For this estimation method, known pilot symbols, which are also called training sequence or preamble, are transmitted. At the receiver end, the channel estimation algorithm operates on the received signal along with its stored symbols to generate an estimate of the transmission channel.
- **Blind Channel Estimation:** This estimation process relies not on training sequence or symbol decisions but rather on certain characteristics of the modulated signal.

In this work, Least Square channel estimation, which is the major data aided channel estimation method, is investigated for its use in M-ary receivers. For the accuracy of the channel estimation, symbol timing information is required. In order to estimate the exact time for the start of the transmitted signal, a frame synchronizer is employed in our work. For a receiver to decode the incoming data stream, the receiver requires to be synchronized with the data streams' frame structure. The frame synchronization is accomplished with the aid of the training data. The receiver knows the training data in the incoming data stream and in the receiver the incoming data stream is correlated with the known training pattern at the known injection interval. The receiver looks for the correlator output where the largest value is attained. Hence, the start time of the incoming symbol is estimated. If the receiver is not in synchronization with the framing pattern, the accumulated correlation is low. Therefore, both the Least Square channel estimator and the frame synchronizer are used in the receiver structure and both of them are based on the transmission of the known preamble data. In this work, the same preamble data, which indeed consists of Kasami sequences, is used for the frame synchronization and the channel estimation.

In this chapter, we first explain the simulated model and then, the performance of the proposed receiver structure is investigated.

5.2 DESCRIPTION OF THE SIMULATED SYSTEM

5.2.1 Channel Model

A wireless channel is a time-varying system in which the parameters are random and liable to change with time. From [2], the equivalent low pass response of the channel is described by its time varying impulse response as follows:

$$h_c(\tau; t) = \sum_n \beta_n(t) e^{-j2\pi f_c \tau_n(t)} \delta(\tau - \tau_n(t)) \tag{5.1}$$

t is the observation instant and $t - \tau$ represents the time where the impulse is applied. $\beta_n(t)$ is the attenuation factor and τ_n is the propagation delay for the n-th path. The multipath channel model is shown in Figure 5.1.

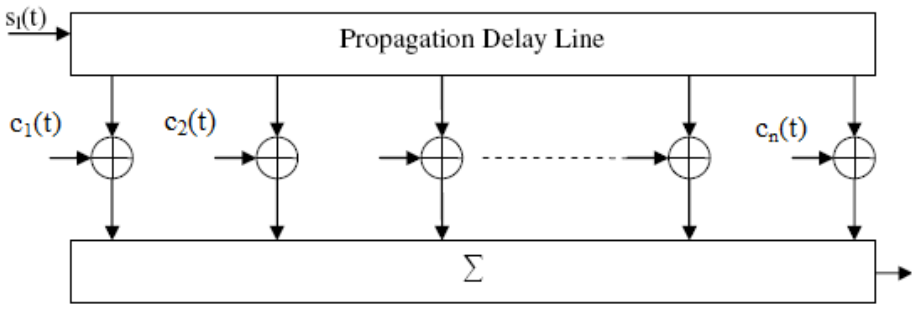

Figure 5.1: Multipath channel model

In order to characterize the multipath channel the scattering function denoted by $S(\tau; f)$ is used. This function procures a measure of the average channel output power as a function of the time delay τ and the Doppler frequency f. Via the scattering function we can get some important characteristics of a channel such as the power delay profile, the power Doppler spectrum which have an impact on the performance of a communication system operating over that channel. In this work, we focus on channels having negligible or no Doppler spread. The power delay profile of the channel which is denoted by $P(\tau)$ is given by

$$P(\tau) = \int S(\tau; f) df \tag{5.2}$$

The power delay profile, also called the multipath intensity profile represents the average power associated with a given multipath delay as a function of the time delay τ. The range of values of τ over which $P(\tau)$ is nonzero is called the multipath spread of the channel and is denoted by T_m. T_m indicates the time dispersive properties of the channel.

COST 207 [20] proposes models for the continuous delay power profile $P(\Delta t)$ for different areas as follows

1. For Rural (Non-hilly) area

$$P(\Delta t) = \begin{cases} e^{-9.2\Delta t} & \text{for } 0 < \Delta t < 7\mu s \\ 0 & \text{elsewhere} \end{cases} \tag{5.3}$$

2. For Urban (Non-hilly) area

$$P(\Delta t) = \begin{cases} e^{-\Delta t} & \text{for } 0 < \Delta t < 7\mu s \\ 0 & \text{elsewhere} \end{cases} \tag{5.4}$$

3. For Hilly Urban area

$$P(\Delta t) = \begin{cases} e^{-\Delta t} & \text{for } 0 < \Delta t < 5\mu s \\ 0.5e^{5-\Delta t} & \text{for } 5 < \Delta t < 10\mu s \\ 0 & \text{elsewhere} \end{cases} \tag{5.5}$$

4. For Hilly Terrain area

$$P(\Delta t) = \begin{cases} e^{-3.5\Delta t} & \text{for } 0 < \Delta t < 2\mu s \\ 0.1e^{15-\Delta t} & \text{for } 15 < \Delta t < 20\mu s \\ 0 & \text{elsewhere} \end{cases} \tag{5.6}$$

Figure 5.2 presents average power delay profiles for corresponding channel types.

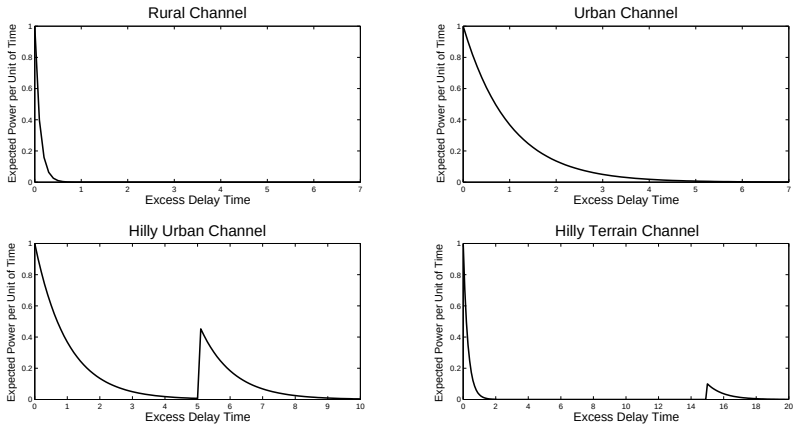

Figure 5.2: Power delay profiles

5.2.2 Simulation Model

The general block diagram for M-ary Kasami code signaling structure has been described in section 2.4.3. In this chapter, the performance of M-ary Kasami code signaling is explored over a multipath fading channel. The packet in each transmission burst is illustrated in Figure

5.3. In simulations, the information data consists of 17 Kasami sequences. Also, Kasami sequences are used as a training data which is used in both the frame synchronization and the LS channel estimation.

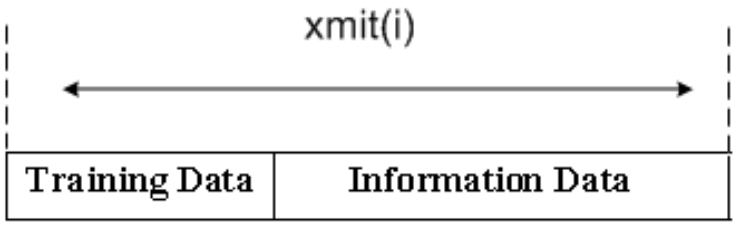

Figure 5.3: Frame structure for a transmission bus

In the simulated model, a tapped delay line (TDL) model of the time invariant frequency selective fading channel is used. The time-invariant equivalent low-pass channel is given by

$$h_c(\tau) = \sum_n h_n \delta(\tau - \tau_n). \tag{5.7}$$

The simulated channel model is shown in Figure 5.4.

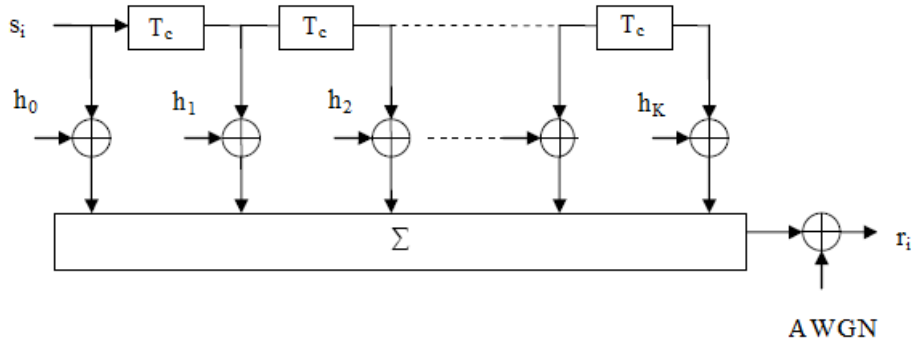

Figure 5.4: Channel model used in simulations

While performing simulations described in this chapter, analog signals involved in the system

diagram are sampled at the chip rate. τ_n is the time delay between the successive taps of the tapped delay line channel model. In simulations, the time delay τ_n is chosen as $\tau_n = T_c$. Since the multipath spread is T_m, the number of taps is $K = (T_m/T_c) + 1$. The tap coefficients h_k are complex, Gaussian, independent random variables with variances σ_k^2 which follows the average power delay profile of the channel and σ_k^2 satisfy the equality:

$$\sum_k \sigma_k^2 = 1 \tag{5.8}$$

in order to normalize the channel average power gain to unity. Tap gains are circularly symetric and Gaussian:

$$h_k = h_{re} + jh_{im} \tag{5.9}$$

where h_{re} and h_{im} are independent and identically distributed Gaussian random variables with mean 0 and variance $\sigma_k/2$.

The simulated receiver model is illustrated in Figure 5.5.

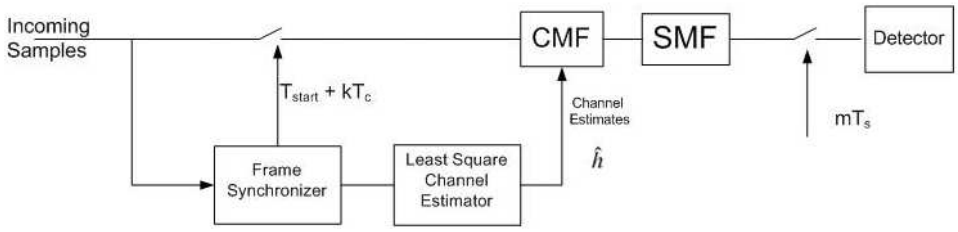

Figure 5.5: Proposed receiver structure

As shown in Figure 5.5, both the frame synchronization and the Least Square channel estimation are performed at the receiver respectively by the aid of a training sequence. Initially, the exact point for the start of the symbol is estimated by the frame synchronizer. The start of the symbol is where the correlation of the training data and the received signal is maximized in a predetermined interval. Then, the Least Square channel estimator follows the synchronizer in order to estimate channel taps. In the absence of the multipath channel the frame synchronizer works fine and gives the exact point for the start of the symbol. However, in the

presence of the multipath channel the frame synchronizer would not give the start time of the incoming symbol correctly since the first path may not be the strongest one. Due to this frame synchronization error, some channel taps can not be estimated. In order to prevent this loss, we consider the start time of the incoming signal T_{start} in terms of the estimated start time T_{frame} which is determined by the frame synchronizer as follows:

$$T_{start} = T_{frame} - 10T_c \tag{5.10}$$

5.3 LEAST SQUARE(LS) CHANNEL ESTIMATION

Least Square (LS) channel estimation approach is the primary approach of channel estimation by using a known training sequence. The LS channel estimation algorithm which aims to minimize the sum of the square of the error is used for the channel estimation over the transmitted pilot sequence. We review the LS algorithm in this section.

Suppose only the training data is transmitted. Then, the received signal $\underline{\mathbf{y}}$ can be expressed as

$$\underline{y} = X\underline{h} + \underline{v} \tag{5.11}$$

where $\underline{\mathbf{h}}$ is the complex channel impulse response, which includes L taps, is denoted by

$$\underline{h} = [h_1 \quad h_2 \quad \dots h_L] \tag{5.12}$$

and X is the training sequence matrix, $\underline{v}$ represents white Gaussian noise. The transmitter sends a training data of P symbols which is denoted by $[x_0 \quad x_1 \quad \dots x_{P-1}]$. The training sequence matrix X is a $P \times L$ matrix given by

$$X = \begin{pmatrix} x_0 & 0 & 0 & \dots & 0 \\ x_1 & x_0 & 0 & \dots & 0 \\ x_2 & x_1 & x_0 & \dots & 0 \\ \vdots & \vdots & \vdots & \vdots & \vdots \\ x_{P-1} & x_{P-2} & x_{P-3} & \dots & x_{P-1-L} \end{pmatrix} \tag{5.13}$$

LS channel estimates are formulated by using the squared error probability:

$$\underline{\hat{h}} = \underset{h}{\operatorname{argmin}} \|y - X\mathbf{h}\|^2 \tag{5.14}$$

Equation 5.14 is solved as follows [14]:

$$\underline{\hat{h}} = (X^H X)^{-1} X^H \underline{y} \tag{5.15}$$

where $()^H$ and $()^{-1}$ denote the Hermitian and inverse matrices, respectively.

Ideally, the training sequence is selected such that the correlation matrix $X^H X$ becomes diagonal. If the correlation matrix is diagonal, equation 5.15 is simplified to

$$\underline{\hat{h}} = \frac{1}{P} X^H \underline{y} \tag{5.16}$$

As a result, channel estimates given by equation 5.16 are simply the correlation between the training sequence and the received signal. The performance of this estimation method is investigated in the following section.

5.4 PERFORMANCE OF LEAST SQUARE CHANNEL ESTIMATION

The LS channel estimator estimates the channel impulse response for each burst separately by using the known training sequence and the received signal. However, invariably, an estimation error occurs during the channel estimation process. Suppose that the estimated channel taps are composed of the exact channel impulse response and the channel estimation error:

$$\underline{\hat{h}} = \underline{h} + \underline{e} \tag{5.17}$$

Due to this estimation error, there will be some unwanted terms in the decision variables.

The received signal is given by

$$y_n = \sum_k h_k I_{n-k} + v_n \tag{5.18}$$

where I_k represent samples belonging to the transmitted symbols and v_n represent noise samples corresponding to AWGN channel. The received signal is passed through the channel matched filter which is based on the channel estimates $\underline{\hat{h}}$ provided by the channel estimator. The channel matched filter output is

$$z_n = (\sum_k h_k I_{n-k} + v_n) * (h^*_{-n} + e^*_{-n}) \tag{5.19}$$

$$z_n = \sum_k (h_k * h^*_{-k}) I_{n-k} + \sum_k (h_k * e^*_{-k}) I_{n-k} + v_n * h^*_{-n} + v_n * e^*_{-n} \tag{5.20}$$

As seen in equation 5.20, the second and fourth terms are undesired terms caused by the channel estimation error. In order to see the effects of these undesired terms, initially the error term is analyzed theoretically. Let R denote the correlation matrix and $R = X^H X$ where X is the training sequence matrix which is shown in equation 5.13. For simulations, Kasami codes are used as a training data and it is known that the cross-correlation function of any two Kasami codes takes small values. Hence the correlation matrix R is approximately diagonal and it is expressed as follows

$$X^H X = R \approx \varepsilon_c N_c I \tag{5.21}$$

where ε_c denotes the chip energy, N_c denotes the training sequence length and I is the identity matrix of size N_c. Then, channel estimates are expressed as

$$\underline{\hat{h}} = R^{-1} X^H \underline{y} = \underline{h} + \underline{e} \tag{5.22}$$

By considering equation 5.18, the channel estimation error is:

$$\underline{e} = R^{-1} X^H \underline{v} \tag{5.23}$$

Then the variance of the channel estimation error is:

$$\sigma_e^2 = (SNR_c \times N_c)^{-1} \tag{5.24}$$

where SNR(Signal to Noise Ratio) per chip is:

$$SNR_c = \frac{\varepsilon_c}{N_0} \tag{5.25}$$

As expressed in equation 5.20, there are two undesired terms due to channel estimation error. It is conjectured that the undesired term, which is related to correlation between the channel estimation error and AWGN channel, has more adverse effects on the system performance. This undesired term is expressed by

$$AWGN \times ChannelEstimationError = v_n * e_{-n}^* \tag{5.26}$$

Suppose this undesired term is denoted by b_n:

$$b_n = \sum_{k=0}^{L} e_k v_{k+n}^* \tag{5.27}$$

Because the channel estimation error and Gaussian noise are independent, the mean square value of b_n is:

$$E\{|b_n|^2\} = \sum_{k=0}^{L} N_0 \sigma_e^2 \tag{5.28}$$

After substituting σ_e^2 in equation 5.28 with an expression given in 5.24, the mean square value of b_n is:

$$E\{|b_n|^2\} = \frac{L \times N_0}{SNR_c \times N_c} \tag{5.29}$$

As seen in equation 5.29, in order to mitigate the effects of the undesired term b_n caused by the correlation between AWGN and the channel estimation error,

- SNR per chip, denoted by $SNR_c = \varepsilon_c / N_0$, should be large or
- L/N_c should be small. That is to say, the length of the training sequence should be much larger than the total channel taps number

$$N_c >> L \tag{5.30}$$

In order to observe the effects of the channel estimation error, simulations are also conducted for different training sequence lengths under Hilly Terrain Channel and a fixed channel with 15 taps. In simulations, the chip duration is chosen as $T_c = 0.1\ \mu sec$. Throughout the simulations, the channel estimation error term and the terms at the channel matched filter output shown in Figure 5.6 are recorded.

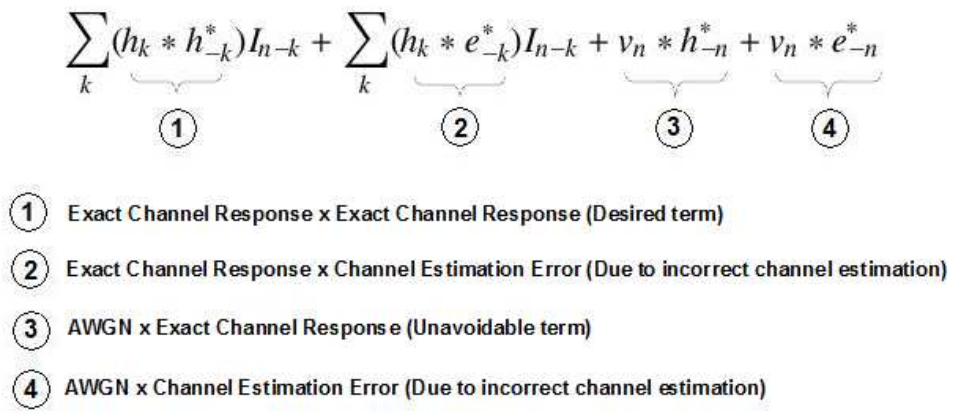

Figure 5.6: Expression at the channel matched filter output

Simulation results are presented in tables 5.1, 5.2, 5.3 and 5.4.

According to simulation results given in these tables, the unwanted term due to the correlation of white Gaussian noise and the channel estimation error becomes effective at the demodulation process. The other unwanted term, caused by the correlation of the channel estimation error and the exact channel response, is also observed in a sufficient amount at the channel matched filter output but the term related to the correlation of white Gaussian noise and the the channel estimation error affects the system more adversely. Also, the simulation results

Table 5.1: Channel estimation performance under Hilly Terrain channel, training sequence length=8×63 chips

$SNRperbit = 5$ dB	Mean	Variance
Channel estimation error e_n	0.0031 - 0.0010i	0.0142
1^{st} term in Figure 5.6	0.0012 - 0.0000i	0.0039
2^{nd} term in Figure 5.6	0.0006 - 0.0010i	0.0062
3^{rd} term in Figure 5.6	0.0171 + 0.0233i	3.9933
4^{th} term in Figure 5.6	0.0277-0.0032	18.2255

Table 5.2: Channel estimation performance under Hilly Terrain channel, training sequence length=32×63 chips

$SNRperbit = 5$ dB	Mean	Variance
Channel estimation error e_n	0.0003 + 0.0002i	0.0044
1^{st} term in Figure 5.6	0.0041 + 0.0000i	0.0038
2^{nd} term in Figure 5.6	-0.0001 + 0.0002i	0.0020
3^{rd} term in Figure 5.6	-0.0484 - 0.0339i	5.7600
4^{th} term in Figure 5.6	-0.0011 + 0.0036i	6.0490

Table 5.3: Channel estimation performance under 15-tapped fixed channel, training sequence length=2×63 chips

$SNRperbit = 5$ dB	Mean	Variance
Channel estimation error e_n	-0.0208 + 0.0593i	0.0508
1^{st} term in Figure 5.6	0.0133 + 0.0000i	0.0097
2^{nd} term in Figure 5.6	-0.0159 - 0.0125i	0.0087
3^{rd} term in Figure 5.6	-0.0470 + 0.0260i	2.9312
4^{th} term in Figure 5.6	0.0804 + 0.0133i	5.0819

Table 5.4: Channel estimation performance under 15-tapped fixed channel, training sequence length=16×63 chips

$SNRperbit = 5$ dB	Mean	Variance
Channel estimation error e_n	0.0201 + 0.0130i	0.0083
1^{st} term in Figure 5.6	0.0133 + 0.0000i	0.0097
2^{nd} term in Figure 5.6	0.0032 - 0.0070i	0.0020
3^{rd} term in Figure 5.6	-0.0026 - 0.0558i	2.8984
4^{th} term in Figure 5.6	-0.0298 - 0.0121i	0.8407

reveal that as the training sequence length gets larger with respect to the number of channel taps, the channel estimation error diminishes and the effects of the undesired terms due to the incorrect channel estimation decrease.

Additionally, these simulation results are compared with the theoretical formulas given in equation 5.24 and 5.29. The related graphs are presented in Figures 5.7, 5.8, 5.9 and 5.10.

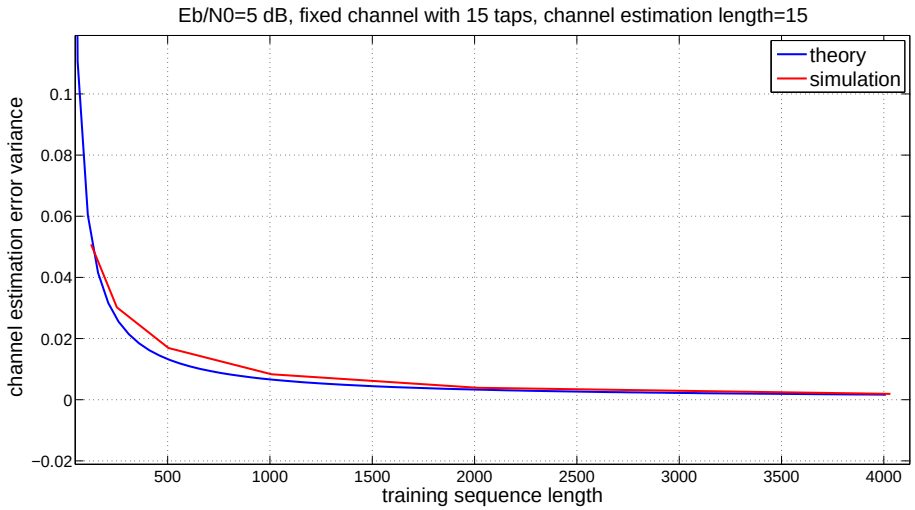

Figure 5.7: Channel estimation error variance for fixed channel

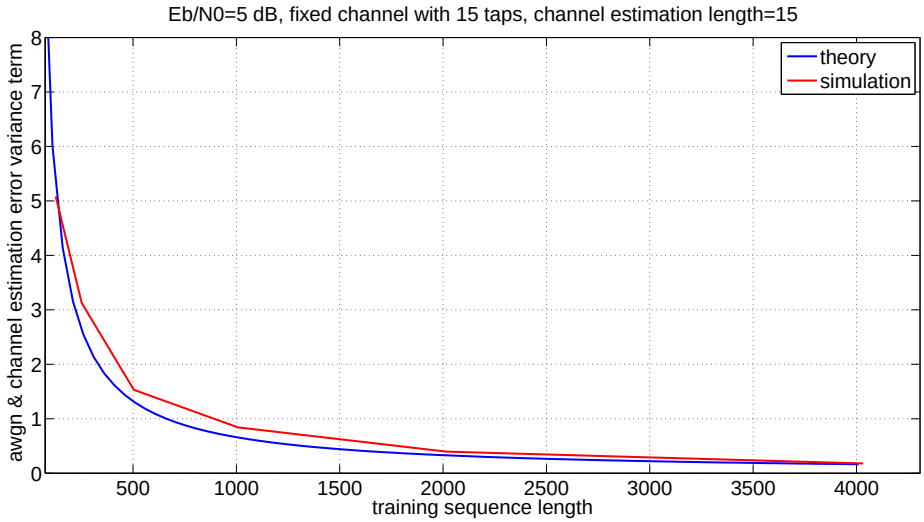

Figure 5.8: AWGN and channel estimation error term variance for fixed channel

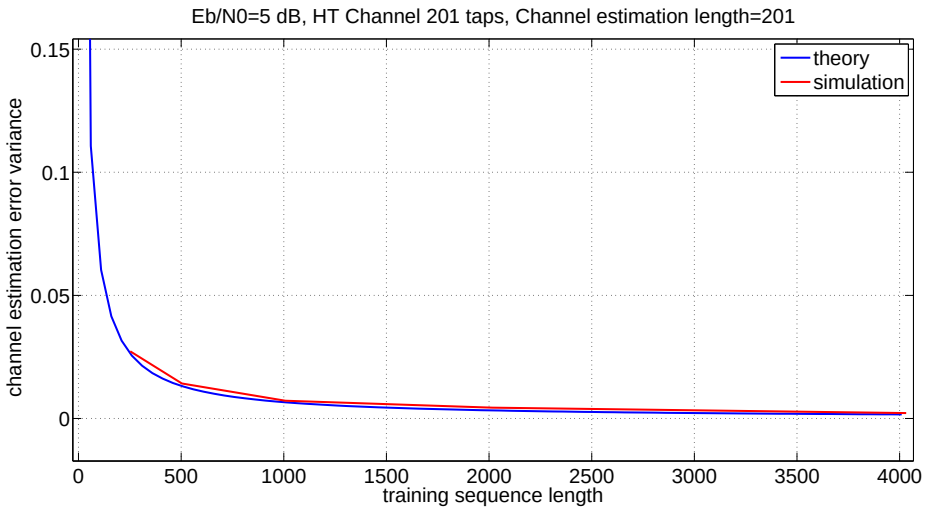

Figure 5.9: Channel estimation error variance for Hilly Terrain channel

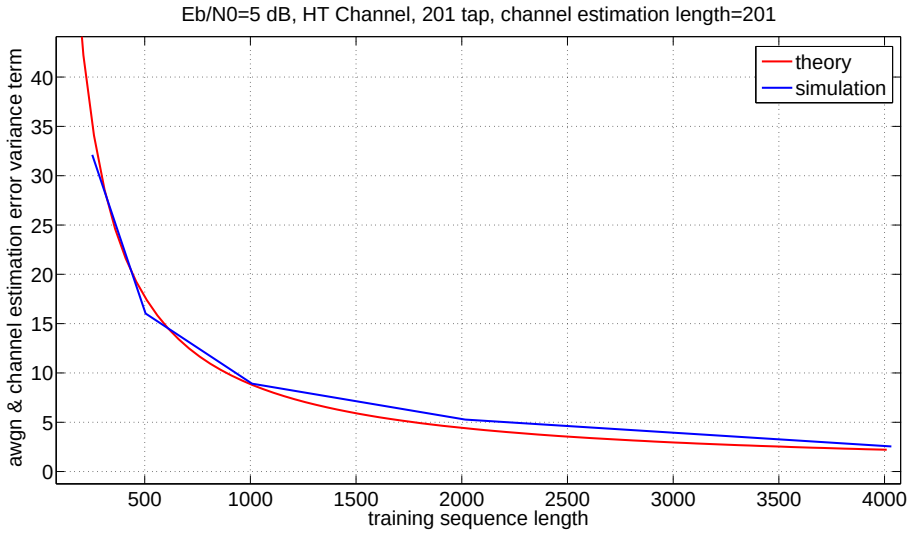

Figure 5.10: AWGN and channel estimation error term variance for HT channel

As seen in Figures 5.7, 5.8, 5.9, 5.10, simulation and theoretical results are approximately the same. A small difference between the simulation and the theoretical results is expected since the correlation matrix R is assumed to be diagonal, but in reality, the correlation matrix R is not exactly diagonal but similar. It is also concluded from the simulation results that as the training sequence length gets larger with respect to the number of channel taps, the channel

estimation error and its effects decrease.

5.5 BER SIMULATIONS AND RESULTS

In this section, the BER performance of the proposed receiver is investigated. The simulation model is as described in section 5.2. Initially, simulations are carried out in order to test the performance of the proposed receiver with a perfect knowledge of the channel parameters. In simulations, COST207 Hilly Terrain channel model is used. As it was mentioned, the multipath spread is $T_m = 20\ \mu sec$ for Hilly Terrain channel. The performance of the receiver is observed for different chip durations $T_c = 10, 1, 0.1, 0.01, 0.001\ \mu sec$ separately. It is known that the total number of taps is $L = T_m/T_c + 1$. Furthermore, for M-ary Kasami code signaling, each symbol consists of 63 chips. The bit error probability of M-ary Kasami code signaling as a function of SNR per bit is illustrated separately for different T_m/T_{symbol} values in Figure 5.11.

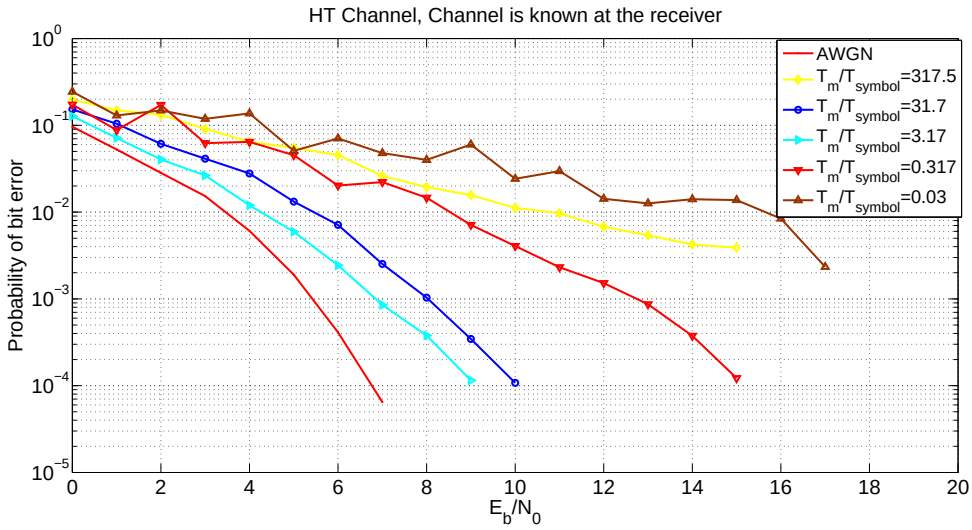

Figure 5.11: Receiver performance under Hilly Terrain channel for different chip rates where the channel characteristic is known at the receiver

The simulation results in Figure 5.11 illustrate the advantage of diversity as a means of overcoming the severe penalty in SNR caused by the multipath fading channel. As seen in Figure 5.11, there is an optimum value T_m/T_{symbol} at which the bit error probability is minimal. A careful examination of these graphs reveals that the minimum bit error rate is obtained when

T_m/T_{symbol} = 3.17. After this optimum value, a degradation in the BER performance is observed. When T_m/T_{symbol} = 317.5, the system performance is degraded dramatically since ISI seriously affects the receiver performance. However, a significant gain in performance is obtained for T_m/T_{symbol} = 31.7 and 3.17. Therefore, it is concluded that even for large values of multipath numbers, M-ary Kasami code signaling still resists inter symbol interference. This indicates the robustness of Kasami codes in a multipath environment.

Now, the performance of the proposed receiver structure including the frame synchronizer and the channel estimator is investigated. Simulations are carried out for the chip rate R_c = 10 Mchip/sec under Hilly Terrain channel. In order to test the proposed receiver, three scenarios are considered.

In the first scenario, the training sequence length is varied for each simulation and the effects of this change on system performance are observed. In this scenario, the channel length is assumed to be known by the receiver. The graphs of bit error rate as a function of SNR per bit are shown in Figure 5.12 for different training sequence lengths.

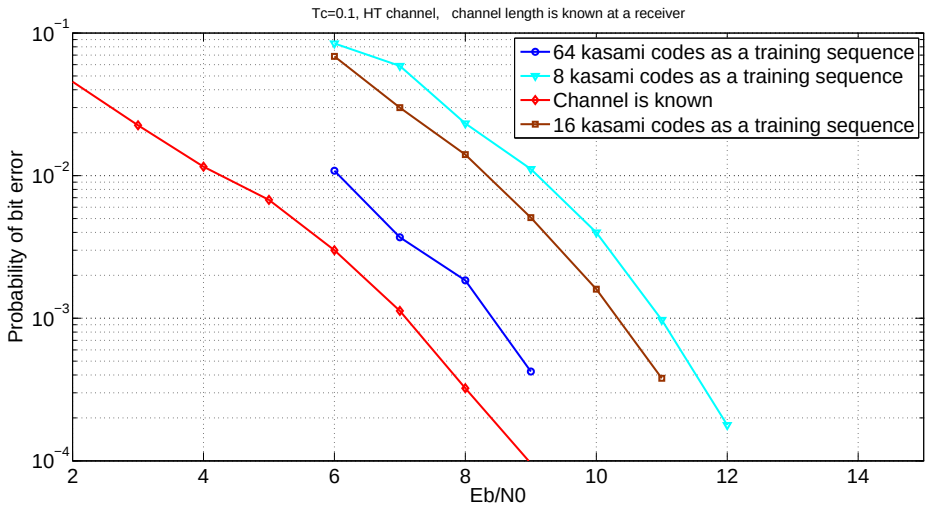

Figure 5.12: Receiver performance for different training sequence lengths under Hilly Terrain channel after the channel estimation algorithm is applied

The simulation results in Figure 5.12 illustrate the improvement in the performance as the training sequence length increases. When the training data consists of 64 Kasami codes, the performance is improved by approximately 2.5 dB with respect to the BER performance

which is obtained by using 8 Kasami codes as a training data. When the training sequence length increases, the channel estimation error decreases and the performance of the proposed receiver is improved.

In the second scenario, the channel length is unknown and the LS channel estimator estimates $\hat{L}$ taps. Simulations are performed under Urban channel and Hilly Terrain channel. The simulation is repeated for different training sequence lengths and the results are compared with the condition in which the channel is known at the receiver. The bit error probability as a function of the number of estimated taps is presented in Figures 5.13, 5.14, 5.15, 5.16 .

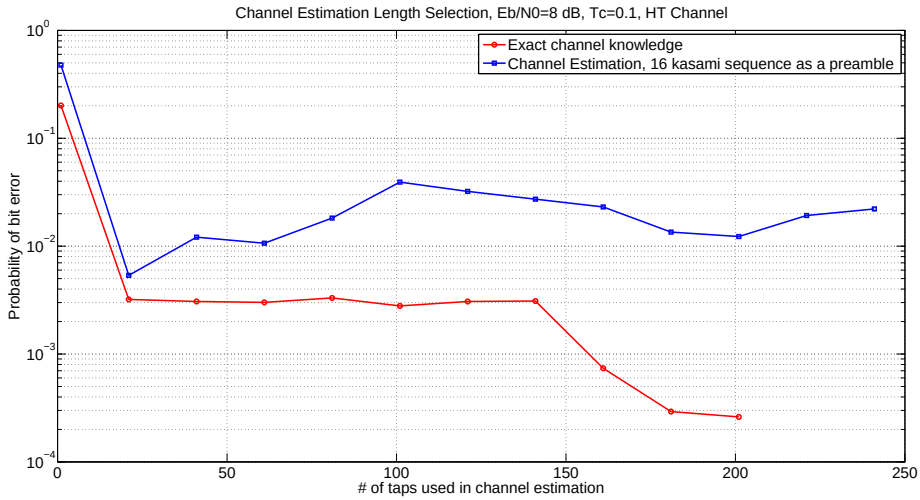

Figure 5.13: Receiver performance under Hilly Terrain channel for different estimated channel lengths

For simulations carried out under Hilly Terrain channel, it seen in Figures 5.13, 5.14 that fluctuations occur in the error rate performance of M-ary signaling while the number of estimated taps $\hat{L}$ increases. For Hilly Terrain channel, there are two separated regions over which the power is spread; together, the spread is much longer for hilly regions as seen in Figure 5.2. Between these two regions, the Hilly Terrain channel includes no taps. However the channel estimator estimates the channel impulse response in case there are nonzero taps. Hence, the noisy taps are estimated to be processed in the channel matched filter which causes the degradation in the performance. As a result, fluctuations in performance are observed due to the

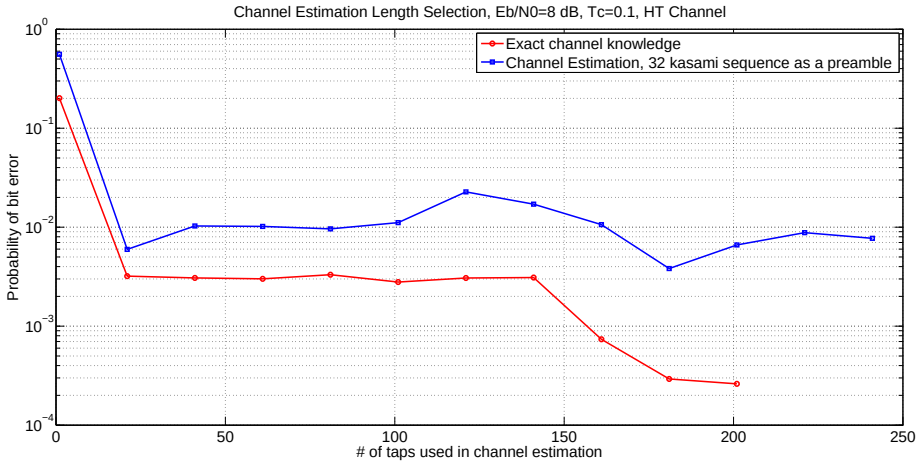

Figure 5.14: Receiver performance under Hilly Terrain channel for different estimated channel lengths

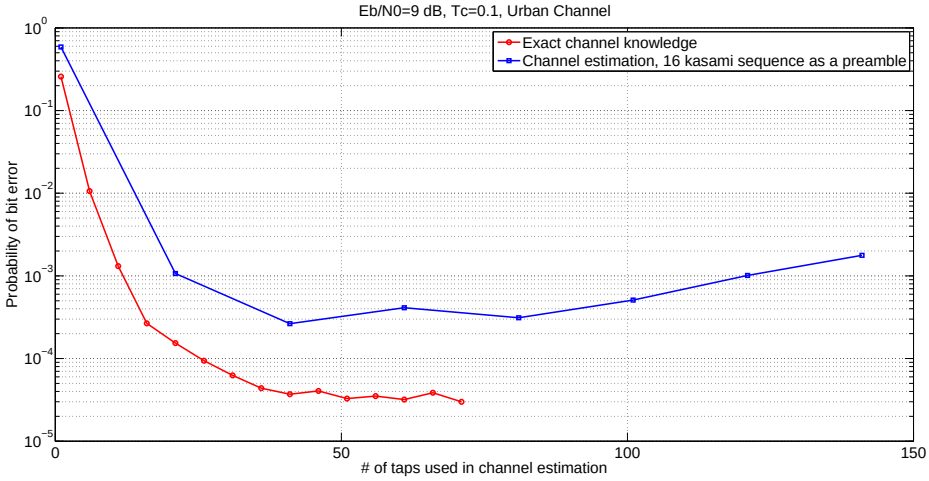

Figure 5.15: Receiver performance for different estimated channel lengths under Urban channel

characteristic of Hilly Terrain channel. For simulations performed under Urban channel, it is seen in Figures 5.15, 5.16 that as the number of estimated taps, $\hat{L}$, gets larger, the performance gets better initially and then the performance is stabilized around a certain value. However, when $\hat{L}$ is larger than the number of exact channel taps, the performance of the estimator decreases, therefore, the system performance is degraded as expected.

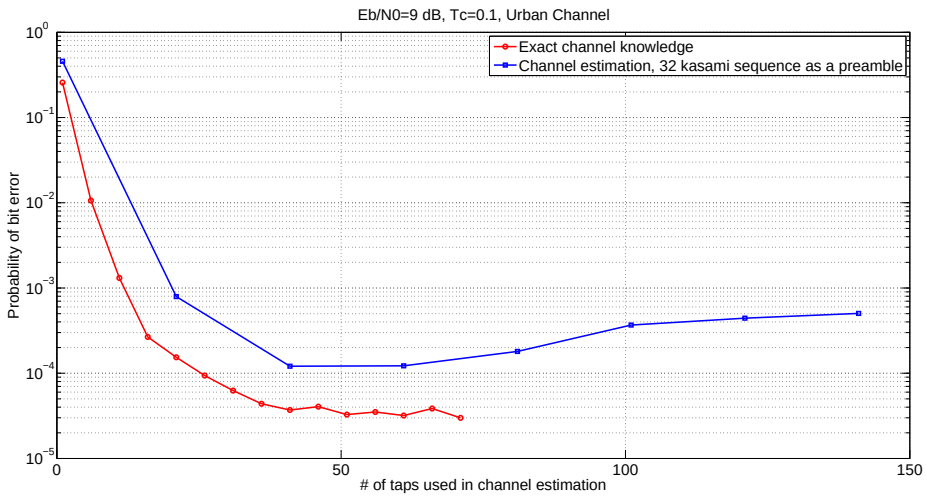

Figure 5.16: Receiver performance for different estimated channel lengths under Urban channel

In the third scenario, it is assumed that the channel length is known at the receiver and the channel estimator selects L_{max} strongest taps from the estimated taps to be processed in the channel matched filter. Since most of the signal energy is concentrated on the strongest taps, it is thought that taking only these into account and not using the weak ones, better performance can be achieved. In the following simulations, Urban channel and Hilly Terrain channel models are used. Simulation results are presented in Figures 5.17, 5.18, 5.19 and 5.20.

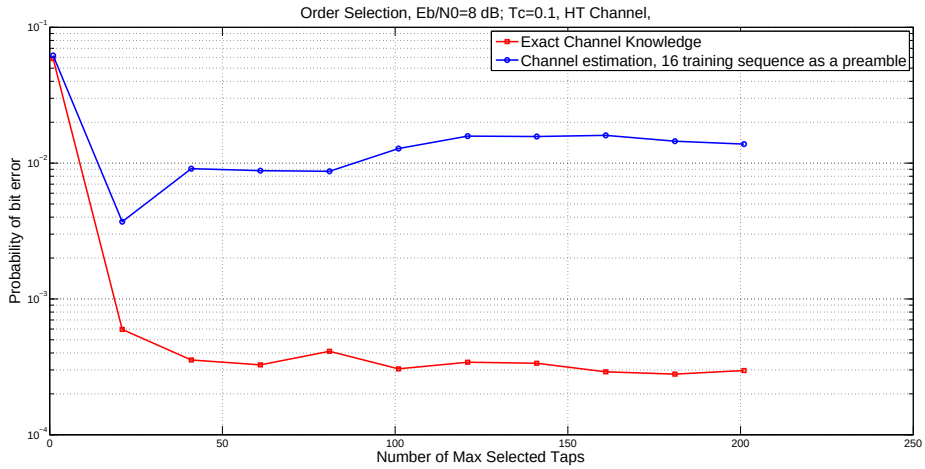

Figure 5.17: Effects of the number of selected strongest taps in channel estimation on the receiver performance under Hilly Terrain channel using 16 Kasami sequences as a training data

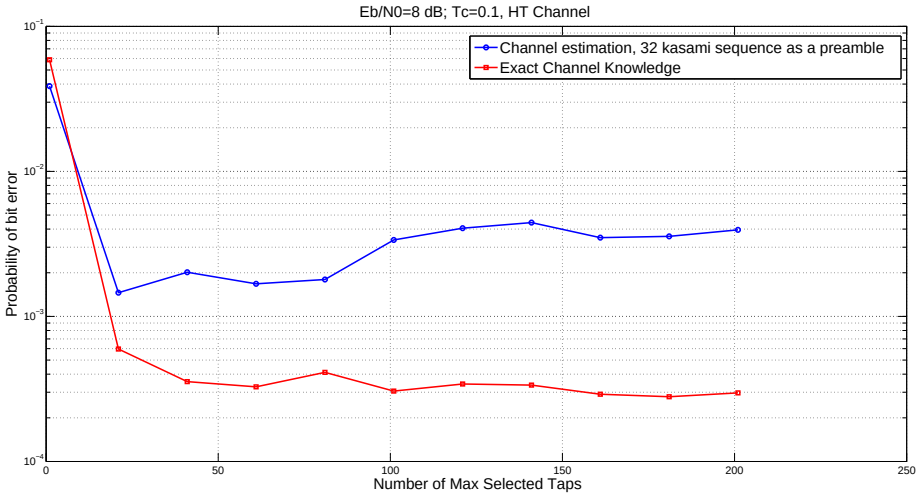

Figure 5.18: Effects of the number of selected strongest taps in channel estimation on the receiver performance under Hilly Terrain channel using 32 Kasami sequences as a training data

As seen in Figure 5.17 and 5.18, the performance gets better until a certain value L_{opt} at which the bit error probability is minimal. When the number of selected strongest taps is greater than L_{opt}, it is concluded that more noisy taps are included in the estimated taps which degrades the receiver performance. The generation of noisy taps in channel estimation is due to the Hilly Terrain channel characteristic.

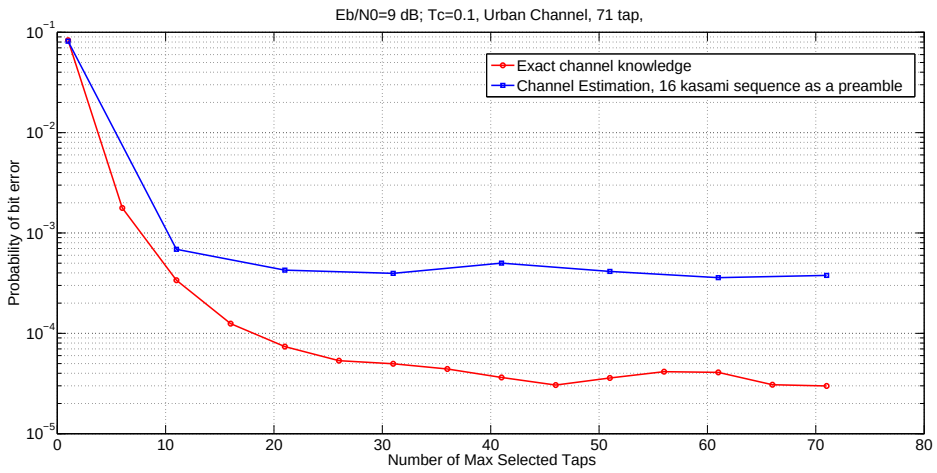

Figure 5.19: Effects of the number of selected strongest taps in channel estimation on the receiver performance under Urban channel using 16 Kasami sequences as a training data

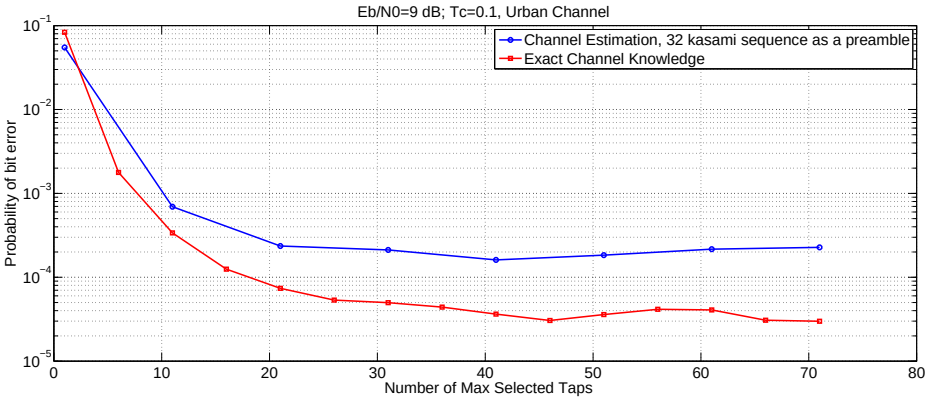

Figure 5.20: Effects of the number of selected strongest taps in channel estimation on the receiver performance under Urban channel using 32 Kasami sequences as a training data

When simulation results for Urban channel in Figure 5.19, 5.20 are observed, it is seen that the BER performance is similar to the case in which the channel is known at the receiver. Furthermore, there is an optimum value L_{opt} after which significant variations in bit error rate of M-ary Kasami code signaling are not observed. It is concluded that most of the channel energy is contained in the L_{opt} strongest channel taps.

CHAPTER 6

CONCLUSIONS

In this thesis study, the performance of M-ary orthogonal modulation has been investigated. For exploring M-ary orthogonal signaling, practical spreading codes have been explored in order to use them in place of orthogonal codes. The analyzed spreading codes are Barker codes, m-sequences, Gold codes, Kasami codes and Walsh-Hadamard codes. Kasami codes are chosen to use in place of orthogonal codes, since they have correlation properties similar to orthogonal codes and they almost satisfy the Welch bound, which is a lower bound on the cross-correlation between any pair of sequences.

For the demodulation process, an optimal receiver structure given in the literature has been used. In the receiver structure, the channel matched filter is utilized to process M-ary signals as a RAKE receiver which is adopted in this study to equalize the channel effects.

Initially, M-ary Kasami code signaling performance is compared with M-ary orthogonal signaling. The results showed that M-ary Kasami code signaling performs better than M-ary orthogonal signaling in terms of bit error rate, since the distance between symbols is increased. The distance is increased because the cross-correlation function of Kasami codes can take negative values. M-ary biorthogonal signaling using Kasami codes has also been examined. It was seen from the results that the advantage of taking negative cross-correlation values for Kasami codes is lost because the absolute value of the matched filter outputs is taken into consideration during the demodulation process. However, M-ary biorthogonal signaling have some advantages over M-ary orthogonal signaling. The data transmission rate for M-ary biorthogonal signaling is higher. In addition, the receiver complexity is reduced for biorthogonal signaling since $M/2$ correlators are sufficient at the receiver.

Secondly, the symbol timing recovery for M-ary signaling has been investigated. A non-

decision directed symbol synchronizer was proposed to estimate the symbol timing. It was seen through simulations that the BER performance of the receiver using the timing provided by the proposed synchronizer is extremely close to that of a receiver operating with exact symbol clock.

Furthermore, the receiver sensitivity to the timing delay has been explored for the transmission of signals over a multipath channel. The simulation results revealed that the receiver is quite insensitive to the symbol timing in the presence of multipath.

The final part of this thesis is on channel estimation to be used in the M-ary receiver. We considered a receiver consisting of a frame synchronizer and channel estimator based on the training sequence operation. The estimated channel is used in the channel matched filter. We have tested the proposed system in COST 207 Hilly Terrain channel and Urban channel environment models. Extensive simulations showed that the system works well even under channel conditions causing significant ISI. We also investigated the use of certain number of the strongest estimated taps instead of the full set of taps. It was seen that this approach can give better performance while reducing the complexity considerably.

The following list provides insight to future work:

- M-ary signaling systems may be investigated for different spreading codes.
- Error detection and correction techniques may be considered. Effects of the usage of error correction codes on the system performance may be explored.
- In this study, BPSK is used. Different digital modulation methods such as QPSK, 8PSK, QAM may be explored on the same framework in M-ary signals.
- MAP channel estimation methods may be applied to estimate the channel impulse response.
- The performance of M-ary Kasami code signaling under carrier frequency offset may be investigated

REFERENCES

[1] Y.Tanık, “M-ary İletim Modelleri”. ODTÜ, EEMB, Haziran 2008.

[2] John G. Proakis, Digital Communications. Fourth Edition. New York: McGraw-Hill, 2001.

[3] Andrea Goldsmith, Wireless Communications. New York: Cambridge University Press, 2005.

[4] Jie Wu, Neng-Jian Tai, Zhi-heng Zhang and Wen-jie Tian, “Performance Analysis of M-ary Multi-Othogonal Keying”, IEEE,2008.

[5] Kumar. V and R. V. Raja Kumar, “Performance Analysis of a Finite Word Length Implemented CCK Modem with Rake Receiver for WLAN System”, The First IEEE and IFIP International Conference in Central Asia on. Vol.26, No.29, Sept. 2005.

[6] George R. Cooper and Clare D. McGillem, Modern Communications and Spread Spectrum. McGraw-Hill, 1986.

[7] S. W. Golomb , Shift Register Sequences. Holden Day, San Francisco, 1967.

[8] S. W. Golomb , Digital Communications with Space Applications. Prentice-Hall,1964.

[9] Esmael H. Dinan and Bijan Jabbari ,“Spreading Codes for Direct Sequence CDMA and Wideband CDMA Cellular Networks”, IEEE Communications Magazine, pp. 48-50, September 1998.

[10] S. Chattopadhyay, S.K:Sanyal, R. Nandi, “Development of Algorithm for the Generation and Correlation Study of Maximal Length Sequences for Applicabilities in CDMA Mobile Communication Systems”.

[11] U. Mengali and A. N. D’Andrea, Synchronization Techniques for Digital Receivers, New York: Plenum Press, 1997.

[12] U. Mengali and A. N. D’Andrea, “The Modified Cramer-Rao Bound and Its Application to Synchronization Problems”,IEEE Transactions on Communications, vol. 42, no. 2/3/4, February/March/April 1994.

[13] H. L. Van Trees, Detection, Estimation and Modulation Theory. New York: Wiley,1968

[14] S. M. Kay, Fundamentals of Statistical Signal Processing: Estimation Theory. Prentice Hall:1998

[15] Fu Li, Xeng Xiao and Jin Yang,“ On Channel Estimation for Rake Receiver In a Mobile Multipath Fading Channel”,IEEE, 1994.

[16] Esmael H. Dinan, Bijan Jabbari, “Spreading Codes for Direct Sequence CDMA and Wideband CDMA Cellular Networks”,IEEE Communication Magazine, September 1998.

[17] Heinrich Meyr, Marc Moeneclaey, Stefan A. Fechtel, Digital Communication Receivers: Synchronization, Channel Estimation and Signal Processing. New York: Wiley,1998.

[18] Tan Wong, Course Notes: Theory of Digital Communications, Chapter 3 Synchronization. Retrieved September 2010 from http://www.dsp.ufl.edu/ twong/Notes/Comm/ch3.pdf

[19] Don Torrieri, Principles of Spread Spectrum Communication Systems. New York: Springer,2005.

[20] M. Failli, Cost 207: Digital Land Mobile Radio Communications. 1989.

[21] Y. Mostofi, D.C.Cox, A. Bahai, "Effect of Frame Synchronization Errors on Pilot-aided Channel Estimation in OFDM: Analysis and Solution". IEEE, 2002.

[22] Yuh-Ren Tsai and Xiu-Sheng Li, "Kasami Code Shift Keying Modulation for Ultra-Wideband Communication Systems",IEEE Transactions on Communications, vol. 55, no. 6, June 2007.

[23] Xiangyong Zeng, John Qingchong Liu and Lei Hu, "Genaralized Kasami Sequences: The Large Set", IEEE Transactions on Information Theory, vol. 53, no. 7, July 2007.

[24] Alan L. Kachelmyer and Keith W. Forsythe , "M-ary Orthogonal Signaling in the Presence of Doppler", IEEE Transactions on Communications, vol. 41, no. 8, August 1993.

[25] L. R. Welch, "Lower Bounds on the Maximum Cross Correlation of Signals", IEEE Transactions on Information Theory, May 1974.

[26] Aki Silvennoinen, "Multipath Propagation and LTV Channel Model", Postgraduate Course in Radio Communications, Autumn 2004.